SANDIA REPORT SAND83—0391 • Unlimited Release • UC—70
Printed December 1983

Interim Report on the Modeling of the Regional Hydraulics of the Rustler Formation

George E. Barr, Warren B. Miller, Don Diego Gonzalez

Prepared by
Sandia National Laboratories
Albuquerque, New Mexico 87185 and Livermore, California 94550
for the United States Department of Energy
under Contract DE-AC04-76DP00789

SF 2900-Q(6-82)

Issued by Sandia National Laboratories, operated for the United States Department of Energy by Sandia Corporation.
NOTICE: This report was prepared as an account of work sponsored by an agency of the United States Government. Neither the United States Government nor any agency thereof, nor any of their employees, nor any of their contractors, subcontractors, or their employees, makes any warranty, express or implied, or assumes any legal liability or responsibility for the accuracy, completeness, or usefulness of any information, apparatus, product, or process disclosed, or represents that its use would not infringe privately owned rights. Reference herein to any specific commercial product, process, or service by trade name, trademark, manufacturer, or otherwise, does not necessarily constitute or imply its endorsement, recommendation, or favoring by the United States Government, any agency thereof or any of their contractors or subcontractors. The views and opinions expressed herein do not necessarily state or reflect those of the United States Government, any agency thereof or any of their contractors or subcontractors.

Printed in the United States of America
Available from
National Technical Information Service
U.S. Department of Commerce
5285 Port Royal Road
Springfield, VA 22161

NTIS price codes
Printed copy: A04
Microfiche copy: A01

SAND83–0391
Unlimited Release
Printed December 1983

Distribution
Category UC–70

Interim Report on the Modeling of the Regional Hydraulics of the Rustler Formation

George E. Barr
Warren B. Miller
Don Diego Gonzalez
Earth Sciences Division 6331
Sandia National Laboratories
Albuquerque, NM 87185

Abstract

The finite-element code ISOQUAD was used to simulate the head distribution within the two major water-bearing units of the Rustler Formation at the Waste Isolation Pilot Plant (WIPP), the Magenta and Culebra dolomites. The derived surfaces correlate well with those generated manually by the US Geological Survey (USGS) and Sandia National Laboratories (SNL). Calculated migration of a continuously injected contaminant from an assumed smeared point source at the center of the site was observed in terms of concentration relative to the initial input. Migration rates of specific concentration fronts decreased with increasing time. The average rate of movement of the 10^{-3} relative concentration contour was less than 10 m/yr for the first 800 yr in the Culebra Dolomite. By 800 yr, the migration of this concentration front has essentially ceased. In the case of the Magenta Dolomite, the average rate of movement of the 10^{-3} relative concentration contour was 0.44 m/yr for the first 676 yr of continuous contaminant injection; the contaminant plume in the Magenta shows little movement thereafter. For reasons of scale, the plume calculation overestimates the actual rate of movement of contaminants. Particle velocities for selected streamlines, more characteristic of contaminant movement, are calculated in Appendix B for comparison with the results of the FEIS. These particle velocities indicate groundwater travel times of ~130 000 yr from the center of the WIPP site to a distance of 12.9 km (8 mi).

The validity of the porous-medium approximation of the Rustler aquifers was examined by the evaluation of the drawdown portion of aquifer pump tests. Drawdown curves were successfully duplicated as a function of hydraulic conductivity, storativity, and well radius. Estimation of the effective radius examined in each well test indicates that there are no significant fluid-bearing fractures or channels within 60 m of tested wells. Because of variable test duration and in situ hydraulic properties, effective radii tested range from 37 to 1500 m (see Appendix A).

Contents

Introduction 7
Fluid Flow Simulation 8
The Magenta and Culebra Dolomite Aquifers 21
  Culebra Unit 21
  Magenta Unit 26
Summary 28
APPENDIX A—Analyses of Supporting Data 29
  Radii of Influence 29
  Interpretation of Single-Well Data 31
    Single-Well Test Reduction 31
    Single-Well Tests 32
      WIPP 25 33
      WIPP 26 34
      WIPP 27 34
      WIPP 28 34
      WIPP 30 36
      P-14 37
      H-7b 37
      H-8b 38
      H-9b 39
  Conclusions for Analyses of Supporting Data 40
  Input for PUMP Code 41
APPENDIX B—Comparison With the Hydraulic Model Used in the FEIS 49
APPENDIX C—Test Problem 53
References 55

Figures

1 Generalized Topographic Map of the Vicinity of the WIPP Site, Including Hole Locations 9
2 Geologic Section Across the WIPP Site 21
3 Areal Assignment of Initial Hydraulic conductivity – K (m/s), and Storativity – s, in the x and y Directions Relative to the Major Transmissivity Tensor for the Culebra Dolomite 22
4 Head Distributions for the Culebra Dolomite, Generated With ISOQUAD, Using Assigned Boundary Conditions and Fixed Values at Wells 24
5 Derived Head Distribution for the Culebra, for the Self-Consistent Problem, With Fixed Boundaries and Varied Assignments of Hydraulic Conductivities 24
6 Initial Plume Configuration in the Culebra Dolomite at Relative Time Zero (time of discovery) 24
7 Plume Migration in the Culebra Dolomite for a Continuous Source Injection of One Unit at the Center of the Site. Concentration points are relative to the unit source, at 21 yr after discovery 24
8 Plume Migration in the Culebra Dolomite for a Continuous Source Injection of One Unit at the Center of the Site. Concentration points are relative to the unit source, at 42 yr after discovery 25
9 Plume Migration in the Culebra Dolomite for a Continuous Source Injection of One Unit at the Center of the Site. Concentration points are relative to the unit source, at 302 yr after discovery 25

Figures (Cont)

10 Plume Migration in the Culebra Dolomite for a Continuous Source Injection of One Unit at the Center of the Site. Concentration points are relative to the unit source, at 468 yr after discovery 25

11 Plume Migration in the Culebra Dolomite for a Continuous Source Injection of One Unit at the Center of the Site. Concentration points are relative to the unit source, at 553 yr after discovery 25

12 Plume Migration in the Culebra Dolomite for a Continuous Source Injection of One Unit at the Center of the Site. Concentration points are relative to the unit source, at 638 yr after discovery 26

13 Plume Migration in the Culebra Dolomite for a Continuous Source Injection of One Unit at the Center of the Site. Concentration points are relative to the unit source, at 808 yr after discovery 26

14 Plume Migration in the Culebra Dolomite for a Continuous Source Injection of One Unit at the Center of the Site. Concentration points are relative to the unit source, at 1405 yr after discovery 26

15 Areal Assignment of Initial Hydraulic Conductivity – K (m/s), and Storativity – s, in the x and y Direction Relative to the Major Transmissivity Tensor for the Magenta Dolomite 27

16 Initial Head Distributions for the Magenta Dolomite, Generated With ISOQUAD, Using Assigned Boundary Conditions and Fixed Values at Wells 27

17 Derived Head Distribution for the Magenta Dolomite for the Self-Consistent Problem, With Fixed Boundaries, and Varied Assignments of Hydraulic Conductivity 27

18 Initial Plume Configuration in the Magenta Dolomite at Relative Time Zero (time of discovery) 28

19 Plume Migration in the Culebra Dolomite for a Continuous Source Injection of One Unit at the Center of the Site. Concentration points are relative to the unit source, at 676 yr after discovery 28

Interim Report on the Modeling of the Regional Hydraulics of the Rustler Formation

Introduction

In modeling work performed in support of the Final Environmental Impact Statment (FEIS) for the Waste Isolation Pilot Plant (WIPP) in southeastern New Mexico, several scenarios involving breach of the facility and resulting in potential release of contaminants to the environment by means of groundwater were investigated, and models were generated for these scenarios. Because of the limited data available at that time (1980), it was necessary to make several assumptions:

- The two fluid-bearing zones within the Rustler Formation, the Magenta and Culebra Dolomites, would form a single composite aquifer, which would be the principal conduit for any releases reaching the environment.
- Both fluid and contaminant-transport modeling of the Rustler Formation could be carried out to a sufficient degree of accuracy by using the porous-medium approximation.
- Ultimate discharge of Rustler brines would occur at Malaga Bend, located along the Pecos River ~39 km (24 mi) from the center of the WIPP site.

Since the FEIS, substantial additional hydrologic data have been collected, which allow development of a more complete model of the flow system in the Rustler. These data indicate the following:

1. There are three separate fluid-bearing units within the Rustler: (a) the Magenta Dolomite, (b) the Culebra Dolomite, and (c) the Rustler-Salado contact. The dolomites are areally extensive and fairly uniform in thickness, each 6.9 to 9 m thick and conforming to the regional dip, generally dipping gently in an easterly direction. The Rustler-Salado interface consists of a dissolution zone within the confines of Nash Draw, but is generally a simple stratigraphic contact elsewhere (Gonzalez, 1983b). The Rustler-Salado contact is not considered as an aquifer in this report, since it is not likely that this local aquifer constitutes a means of transporting contaminants in the vicinity of the WIPP.
2. In most areas, the relative and absolute values of freshwater heads in the Magenta and Culebra Dolomites are separate and distinct. For the most part, head potentials decrease downwards within the Rustler, with those in the Magenta generally higher than those in the Culebra and those in the Culebra higher than those in the Rustler-Salado interface.
3. In addition, it appears that fluids from the underlying Bell Canyon could just reach the elevation of the Culebra in an open hole. It may be that, in the event of any connection between the two aquifer zones, flow would actually be downwards, rather than upwards into the Culebra or Magenta. However, since the data for the Bell Canyon are scanty at present, it is presumed here (in order for fluids to move more quickly to the biosphere) that the primary units for solute transport at the WIPP remain the Magenta and Culebra.

The main objectives of this report are to

1. Numerically simulate the separate freshwater potential surfaces within the Magenta and Culebra Dolomites
2. Estimate the rates and extents of migration of ideally nonsorbing contaminants continuously injected into the Culebra and Magenta Dolomites

Supporting analyses have been placed in appendices, rather than in the general text. Appendix A investigates in detail the drawdown responses of several pumped wells at and near the WIPP. The goal is to reexamine the validity of the porous-medium approximation in modeling Rustler hydraulics. Appendix B compares groundwater travel times calculated

here with those estimated in the FEIS. The objective is to determine whether or not the FEIS calculations still appear conservative. Appendix C compares model results obtained here in a test problem with those contained in a primary reference.

Fluid Flow Simulation

Pump tests performed both on three-hole hydro pads and in individual hydro holes are compared against pump tests calculated by using the porous-medium approximation in Appendix A. Results contained in Appendix A indicate that

- In most cases pump tests at and near WIPP can be adequately represented through use of a porous-medium approximation.
- Radii of influence, within which significant high-permeability channels are absent, range from 37 to 1500 m (120 and 5000 ft) depending on the well tested.

Based on these results, it is assumed in following discussions that the porous-medium approximation is an adequate representation of Rustler hydraulics.

To simulate movement of fluids in the Magenta and Culebra Units, a mathematical representation is needed of such flow and of the fluid-bearing units. The representation used here consists of the appropriate differential equations and a grid representing the region of interest. The Culebra and Magenta Dolomites being saturated, artesian, and of uniform thicknesses throughout the study area, it is expedient to represent each unit in two dimensions. In this case an areal representation is chosen that greatly reduces time and expense of computation. The area in which flow is simulated is a block 25.8 × 25.8 km (16 × 16 mi) centered on the proposed site. This area was picked to include almost all of the available hydrologic study holes and most of the area of Nash Draw located west of the site (see Figure 1). The entire area was broken down into blocks 1.6 km (1 mi) square, a grid size chosen to be consistent with both the radii of influence obtained for the various experimental hydrologic study holes and with the general spacing of the study holes.

The following equations were developed by integrating the more general three-dimensional forms over the vertical dimensions.

The equations to be solved are

1. $$\nabla \cdot (\epsilon D \cdot \nabla C) - \nabla \cdot (Cq) - \frac{\partial}{\partial t}(C\epsilon b) - b\epsilon C\alpha_p \delta g \cdot \frac{\partial h}{\partial t} - C\overline{W} - C_\ell \frac{K\ell}{b_\ell}(h - h_\ell) = 0$$

2. $$q + \overline{T} \cdot \nabla h = 0$$

3. $$\overline{S}\frac{\partial h}{\partial t} + \nabla \cdot (\delta q) + \epsilon b \beta_d \frac{\partial c}{\partial t} - \delta \overline{W} - \delta_\ell \frac{K_\ell}{b_\ell} \cdot (h - h_\ell) = 0 \quad ,$$

where

b	=	thickness of the aquifer (L)
C	=	the mass concentration of the contaminant in the fluid (M/L^3)
D	=	bD′ is an effective dispersion coefficient for the entire thickness b of the aquifer, and D′ is the dispersion tensor (L^3/T)
q	=	the mass average-rate of flow per unit width of the aquifer (L^2/T)
$\overline{S}$	=	$\delta g b \Delta$ is a dimensionless storage coefficient (Δ = coefficient of storativity)
$\overline{T}$	=	the transmissivity tensor (L^2/T)
$\overline{W}$	=	bW, where W is the rate of production of a source or sink $\left(\frac{L}{T}\right)$
ϵ	=	the porosity
h	=	head (L)
δ	=	fluid density (M/L^3)
δ	=	$\delta_o + \beta_d(C\text{-}Co)$, fluid density ($M/L^3$)
α_p	=	coefficient of compressibility
β_d	=	coefficient for dependence of density on concentration
χ_ℓ	=	corresponding quantities for the overlying confining aquifer are subscripted ℓ
g	=	gravitational constant (L/T^2)

The equations were solved by using an existing computer code (ISOQUAD) (Pinder, 1974), a finite-element code in two dimensions, used for simulating flows in a porous medium. The method of solution in ISOQUAD utilizes the Galerkin technique. This code is for isothermal flow, and assumes no density change in the fluid due to the presence of the contaminants. The operation of the code was tested by running a test problem from the literature, documented in Appendix C, which exhibits a well-formed plume and is supported by field data (Pinder, 1973). For the calculations, a finite-element grid was first set up, consisting of a 25.76 km-(16 mi-) square array of 256 elements, 16 × 16, with a total of 367 nodal points. The center of the repository site is located at the center of the grid.

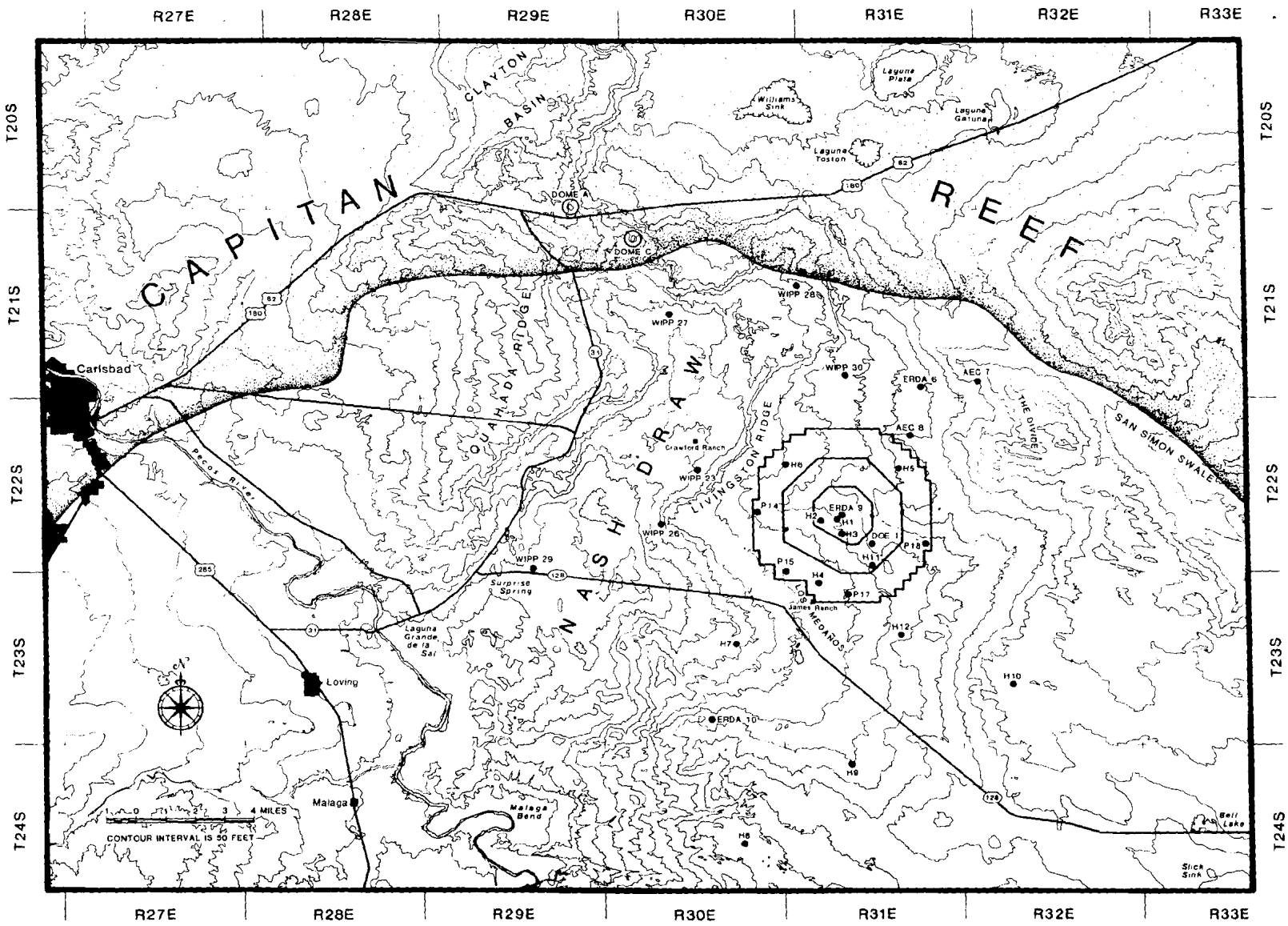

Figure 1. Generalized Topographic Map of the Vicinity of the WIPP Site, Including Hole Locations

The boreholes for hydraulic testing are shown in Figure 1 (Gonzalez, 1983a). Since this is an inverse problem (Anderson, 1979) without a known head structure, it is necessary to first establish an initial head distribution. From that, a distribution of hydraulic conductivities and boundary conditions can be derived to allow construction of a self-consistent model that reproduces the experimental head values. Construction of that model includes a variation of parameters to investigate the sensitivity of the head distribution to the values selected. To establish a head distribution in the grid, the exterior boundary of the grid was made a reflection boundary, and head values determined at the boreholes were set as fixed-boundary values. Nodal points were moved to correspond with the locations of individual wells. The results, however, are plotted on a rectangular grid. Values for porosity, transmissivity, and aquifer thickness for each element were established on the basis of existing borehole hydraulic data (Gonzales, 1983a), stratigraphy (Powers et al, 1978), and local hydraulic trends (decreasing transmissivity from west to east across the proposed WIPP site in the Culebra (Gonzalez, 1983b)), Figures 3 and 15. Elements containing a test borehole or in the immediate vicinity of a borehole are assigned values determined by tests at that borehole. Average values were assigned for unknown parameters, based on the stratigraphic trends and the closest available borehole data. Because of the head differential between the Culebra and Magenta (except in part of Nash Draw) it was assumed that there was no vertical leakage. Based on the derived head distribution, Figures 4 and 16, and the assumed distribution of hydraulic conductivities, K, a self-consistent set of K's and heads was established (i.e., Figures 5 and 17). In this process the heads were fixed at the boundary and the values of K varied to attempt to match the experimental head values at the wells; the match is shown in Figures 5 and 17. The variations were done with the following premises: (1) variation of K should as much as possible be within the range of measurements, (2) drastic changes of K are avoided unless supported by near-by well data, (3) boundary values of the head are adjusted when (1), (2) are unsuccessful, and (4) there should be a reasonable approximation to the known head values. The derived K distributions for the self-consistent problem are given in Tables 1 and 2 for the Culebra and Magenta, respectively; the values vary from the initial values on an element-by-element basis. The element count starts by columns in the lower left corner and counting vertically upwards to 256. For the calculation of plume migration, the exterior boundary was made a Dirichlet boundary for heads and concentration; contaminant concentration was set at zero at the boundaries.

After the calculation of the self-consistent potentiometric head distribution, the next step was to reduce the scale of the problem being calculated so that the motion of a mass of contaminant, a plume, could be calculated in more detail. Three "cutouts" of the center of the region around the site were made, 9.68 × 9.68 km (6 × 6 mi), 4.8 × 4.8 km (3 × 3 mi), and 2.4 × 2.4 km (1.5 × 1.5 mi) in size. The head distributions derived in the large problem (16 × 16 mi) were assigned to each of the smaller regions. The smallest cutout consisted of 256 elements, 150 × 150 m (492 × 492 ft) in size.

The problem of contaminant migration was started in the smallest scale (2.4 × 2.4 km), using a fixed, constant source of one unit at the center, and arbitrarily assigning a relative concentration of 0.1 to the nodes immediately surrounding the point source. A Dirichlet boundary condition for concentration was applied at the boundaries and set to zero. The motion of this initial plume is calculated until the time at which the plume begins to interact with the model boundary. At that time, the results are transferred to the next larger cutout (4.8 × 4.8 km), so that the boundary is moved farther away from the source of the contaminants, and calculations are resumed. This procedure is continued, as necessary, to the large problem, in order to minimize interaction with the boundary of the model.

Even though a sharp, well-defined plume is input into the smallest problem, dispersion, resulting from physical processes, the numerical method used and the change of scale cause the plume's edges to become less distinct with increasing time. This means that there is not a sharp contaminant front, so the results of the calculations are displayed in terms of specific fractions of the initial source input. In these calculations, the relative concentrations plotted are 10^{-1}, 10^{-2}, and 10^{-3} of the source input.

A unit source is specified so that a wide range of release scenarios and types of contaminants is included. This input source runs continually for the duration of the calculations. It is not obvious that the inventory of WIPP for a given nuclide is exhausted by the time of the last run presented here (0.7×10^3 to 1.4×10^3 yr). To correct the unit source assumed in the calculations to an actual concentration requires specification of the chemical state of the fluid and the contaminant.

Table 1. Derived Values for the Hydraulic Conductivity of the Head Distribution: Culebra Unit

ELEMENT NUMBER	HYDRAULIC CONDUCTIVITY (m/sec) (X)	(Y)	STORAGE	POROSITY
1	2.57E-05	5.90E-05	1.0E-05	.100
2	2.57E-05	5.90E-05	1.0E-05	.100
3	2.57E-05	5.90E-05	1.0E-05	.100
4	2.57E-05	5.90E-05	1.0E-05	.100
5	2.17E-05	5.00E-05	1.0E-05	.100
6	2.17E-05	5.00E-05	1.0E-05	.100
7	2.17E-05	5.00E-05	1.0E-05	.100
8	2.17E-05	5.00E-05	1.0E-05	.100
9	2.17E-05	5.00E-05	1.0E-05	.100
10	2.17E-05	5.00E-05	1.0E-05	.100
11	2.17E-05	5.00E-05	1.0E-05	.100
12	2.17E-05	5.00E-05	1.0E-05	.100
13	2.17E-05	5.00E-05	1.0E-05	.100
14	2.17E-05	5.00E-05	1.0E-05	.100
15	2.17E-05	5.00E-05	1.0E-05	.100
16	1.43E-05	3.30E-05	1.0E-06	.100
17	2.57E-05	5.90E-05	1.0E-05	.100
18	2.57E-05	5.90E-05	1.0E-05	.100
19	2.57E-05	5.90E-05	1.0E-05	.100
20	2.57E-05	5.90E-05	1.0E-05	.100
21	2.17E-05	5.00E-05	1.0E-05	.100
22	2.17E-05	5.00E-05	1.0E-05	.100
23	2.17E-05	5.00E-05	1.0E-05	.100
24	2.17E-05	5.00E-05	1.0E-05	.100
25	2.17E-05	5.00E-05	1.0E-05	.100
26	1.06E-05	2.44E-05	1.0E-02	.100
27	1.06E-06	2.44E-06	1.0E-02	.100
28	2.17E-06	5.00E-06	1.0E-05	.100
29	2.17E-05	5.00E-05	1.0E-05	.100
30	2.17E-05	5.00E-05	1.0E-00	.100
31	2.17E-05	5.00E-05	1.0E-05	.100
32	2.17E-05	5.00E-05	1.0E-05	.100
33	4.42E-05	1.02E-04	3.0E-04	.100
34	4.42E-05	1.02E-04	3.0E-04	.100
35	4.42E-05	1.02E-04	3.0E-04	.100
36	4.42E-05	1.02E-04	3.0E-04	.100
37	3.33E-05	7.67E-05	1.0E-05	.100
38	3.33E-05	7.76E-05	1.0E-05	.100
39	2.00E-05	4.60E-05	1.0E-05	.100
40	2.00E-05	4.60E-05	1.0E-05	.100
41	1.06E-05	2.43E-05	1.0E-02	.100
42	1.06E-05	2.43E-05	1.0E-02	.100
43	1.06E-05	2.44E-05	1.0E-02	.100
44	1.00E-05	2.30E-05	1.0E-05	.100
45	2.00E-05	4.60E-05	1.0E-05	.100
46	2.86E-05	6.60E-05	1.0E-06	.100
47	1.43E-05	3.30E-05	1.0E-06	.100
48	1.43E-05	3.30E-05	1.0E-06	.100
49	4.42E-05	1.02E-04	3.0E-04	.100
50	4.42E-05	1.02E-04	3.0E-04	.100
51	4.42E-05	1.02E-04	3.0E-04	.100
52	4.42E-05	1.02E-04	3.0E-04	.100
53	3.33E-05	7.67E-05	1.0E-05	.100
54	3.33E-05	7.67E-05	1.0E-05	.100
55	2.00E-05	4.60E-05	1.0E-05	.100
56	2.00E-05	4.60E-05	1.0E-05	.100

>?

DISPERSIVITY (m) LONGITUDINAL	TRANSVERSE
20.0	2.0

FOR ALL ELEMENTS

(INTERA, 1981)

Table 1. (cont)

ELEMENT NUMBER	HYDRAULIC CONDUCTIVITY (m/sec) (X)	(Y)	STORAGE	POROSITY
57	2.00E-05	4.60E-05	1.0E-05	.100
58	2.00E-05	4.60E-05	1.0E-05	.100
59	1.77E-05	4.06E-05	0.5E-02	.100
60	1.77E-05	4.06E-05	0.5E-02	.100
61	1.70E-05	3.30E-05	1.0E-05	.100
62	2.86E-05	6.60E-05	1.0E-06	.100
63	2.86E-05	6.60E-05	1.0E-06	.100
64	1.43E-05	3.30E-05	1.0E-06	.100
65	4.42E-05	1.02E-04	3.0E-04	.100
66	4.42E-05	1.02E-04	3.0E-04	.100
67	4.42E-05	1.02E-04	3.0E-04	.100
68	4.42E-05	1.02E-04	3.0E-04	.100
69	0.53E-05	1.23E-06	1.0E-05	.100
70	1.17E-06	2.69E-06	1.0E-05	.100
71	1.12E-08	4.88E-09	1.0E-04	.100
72	1.12E-08	4.88E-09	1.0E-04	.100
73	3.31E-05	7.62E-05	0.1E-04	.100
74	3.31E-05	7.62E-05	0.1E-04	.100
75	1.77E-05	4.06E-05	0.5E-02	.100
76	1.77E-05	4.06E-05	0.5E-02	.100
77	1.43E-05	3.30E-05	1.0E-05	.100
78	1.43E-05	3.30E-05	1.0E-06	.100
79	1.43E-05	3.30E-05	1.0E-06	.100
80	1.43E-05	3.30E-05	1.0E-06	.100
81	4.42E-05	1.02E-04	3.0E-04	.100
82	4.42E-05	1.02E-04	3.0E-04	.100
83	4.42E-05	1.02E-04	3.0E-04	.100
84	4.42E-05	1.02E-04	3.0E-04	.100
85	2.17E-06	5.00E-05	1.0E-05	.100
86	2.30E-07	1.00E-07	6.0E-06	.100
87	1.12E-08	4.88E-09	1.0E-04	.100
88	1.12E-08	4.88E-09	1.0E-04	.100
89	3.31E-05	7.62E-05	1.0E-05	.100
90	3.31E-05	7.62E-05	1.0E-05	.100
91	2.17E-05	5.00E-05	1.0E-05	.100
92	2.17E-05	5.01E-05	1.0E-05	.100
93	2.17E-05	5.01E-05	1.0E-05	.100
94	1.43E-05	3.30E-05	1.0E-06	.100
95	1.43E-05	3.30E-05	1.0E-06	.100
96	1.43E-05	3.30E-05	1.0E-06	.100
97	4.42E-05	1.02E-04	0.3E-03	.100
98	4.42E-05	1.02E-04	0.3E-03	.100
99	4.42E-05	1.02E-04	0.3E-03	.100
100	4.42E-05	1.02E-04	3.0E-04	.100
101	1.41E-07	6.10E-08	1.0E-06	.100
102	1.41E-07	6.17E-08	1.0E-06	.100
103	2.30E-07	1.00E-07	6.0E-06	.100
104	0.25E-07	0.56E-07	1.0E-05	.100
105	0.49E-07	1.13E-07	1.0E-05	.100
106	4.61E-06	1.06E-05	1.0E-05	.100
107	4.60E-06	1.06E-05	2.0E-05	.100
108	1.43E-05	3.30E-05	2.0E-05	.100
109	1.43E-05	3.30E-05	1.0E-05	.100
110	1.43E-05	3.30E-05	1.0E-06	.100
111	1.43E-05	3.30E-05	1.0E-06	.100
112	1.43E-05	3.30E-05	1.0E-06	.100

>?

DISPERSIVITY (m) LONGITUDINAL	TRANSVERSE
20.0	2.0

FOR ALL ELEMENTS

(INTERA, 1981)

Table 1. (cont)

ELEMENT NUMBER	HYDRAULIC (m/sec) CONDUCTIVITY (X)	(Y)	STORAGE	POROSITY
113	4.42E-05	1.02E-04	0.3E-03	.100
114	4.42E-05	1.02E-04	0.3E-03	.100
115	4.42E-05	1.02E-04	0.3E-03	.100
116	4.42E-05	1.02E-04	3.0E-04	.100
117	1.41E-07	0.61E-07	1.0E-06	.100
118	1.41E-07	6.10E-08	1.0E-06	.100
119	0.63E-07	1.44E-07	1.0E-05	.100
120	0.20E-08	0.46E-08	1.0E-05	.100
121	4.90E-09	1.13E-08	1.0E-05	.100
122	2.17E-07	5.00E-07	1.0E-05	.100
123	4.60E-06	1.06E-05	2.0E-05	.100
124	1.38E-05	3.18E-05	2.0E-05	.100
125	1.38E-05	3.18E-05	1.0E-05	.100
126	1.38E-05	3.18E-05	1.0E-05	.100
127	1.21E-05	2.79E-05	1.0E-01	.100
128	1.21E-05	2.79E-05	1.0E-01	.100
129	4.42E-05	1.02E-04	0.3E-03	.100
130	4.42E-05	1.02E-04	0.3E-03	.100
131	4.42E-05	1.02E-04	0.3E-03	.100
132	4.42E-05	1.02E-04	3.0E-04	.100
133	1.41E-07	0.61E-07	1.0E-05	.100
134	1.41E-07	0.61E-07	1.0E-05	.100
135	1.26E-07	2.89E-07	1.0E-05	.100
136	0.61E-08	1.40E-08	1.0E-05	.100
137	0.46E-08	1.06E-08	1.0E-05	.100
138	2.17E-08	5.00E-08	1.0E-05	.100
139	2.17E-08	5.00E-08	1.0E-05	.100
140	2.17E-06	5.00E-06	1.0E-05	.100
141	1.38E-05	3.18E-05	1.0E-05	.100
142	1.21E-05	2.79E-05	1.0E-01	.100
143	1.21E-05	2.79E-05	1.0E-01	.100
144	1.21E-05	2.79E-05	1.0E-01	.100
145	3.46E-09	7.97E-09	1.0E-04	.100
146	3.46E-09	7.97E-09	1.0E-04	.100
147	3.46E-09	7.97E-09	1.0E-04	.100
148	3.46E-09	7.97E-09	1.0E-04	.100
149	2.17E-09	5.00E-09	1.0E-05	.100
150	5.29E-11	1.22E-10	1.0E-05	.100
151	5.29E-11	1.22E-10	1.0E-05	.100
152	0.46E-08	1.06E-08	1.0E-05	.100
153	9.33E-09	2.15E-08	2.0E-05	.100
154	9.33E-09	2.15E-08	2.0E-05	.100
155	1.54E-07	2.52E-07	1.0E-05	.100
156	1.33E-06	3.05E-06	1.0E-04	.100
157	1.33E-05	3.05E-05	1.0E-04	.100
158	1.21E-05	2.79E-05	1.0E-01	.100
159	1.21E-05	2.79E-05	1.0E-01	.100
160	1.21E-05	2.79E-05	1.0E-01	.100
161	3.46E-09	7.97E-09	1.0E-04	.100
162	1.73E-09	3.98E-09	1.0E-04	.100
163	3.46E-09	7.97E-09	1.0E-04	.100
164	3.46E-09	7.97E-09	1.0E-04	.100
165	2.17E-09	5.00E-09	1.0E-05	.100
166	5.29E-11	1.22E-10	1.0E-05	.100
167	5.29E-11	1.22E-10	1.0E-05	.100
168	1.50E-09	2.52E-09	1.0E-05	.100

>?

DISPERSIVITY (m) LONGITUDINAL	TRANSVERSE
20.0	2.0

FOR ALL ELEMENTS

(INTERA, 1981)

Table 1. (cont)

ELEMENT NUMBER	HYDRAULIC CONDUCTIVITY (m/sec) (X)	(Y)	STORAGE	POROSITY
169	9.33E-09	2.15E-08	2.0E-05	.100
170	9.33E-09	2.15E-08	2.0E-05	.100
171	1.54E-08	2.52E-08	1.0E-05	.100
172	1.33E-06	3.05E-06	1.0E-04	.100
173	1.33E-06	3.05E-06	1.0E-04	.100
174	1.21E-05	2.79E-05	1.0E-01	.100
175	1.21E-05	2.79E-05	1.0E-01	.100
176	1.21E-05	2.79E-05	1.0E-01	.100
177	3.46E-09	7.97E-09	1.0E-04	.100
178	1.73E-09	3.98E-09	1.0E-04	.100
179	3.46E-09	7.97E-09	1.0E-04	.100
180	3.46E-09	7.97E-09	1.0E-04	.100
181	2.17E-08	5.00E-08	1.0E-05	.100
182	2.17E-08	5.00E-08	1.0E-05	.100
183	0.61E-10	1.41E-10	1.0E-05	.100
184	0.61E-10	1.41E-10	1.0E-05	.100
185	2.17E-08	5.00E-08	1.0E-05	.100
186	2.17E-08	5.00E-08	1.0E-05	.100
187	2.17E-08	5.00E-08	1.0E-05	.100
188	1.54E-06	2.52E-06	1.0E-05	.100
189	2.17E-06	5.00E-06	1.0E-05	.100
190	2.17E-05	5.00E-05	1.0E-05	.100
191	2.17E-05	5.00E-05	1.0E-05	.100
192	2.17E-05	5.00E-05	1.0E-05	.100
193	3.46E-09	7.97E-09	1.0E-04	.100
194	3.46E-09	7.97E-09	1.0E-04	.100
195	3.46E-09	7.97E-09	1.0E-04	.100
196	3.46E-09	7.97E-09	1.0E-04	.100
197	2.17E-08	5.00E-08	1.0E-05	.100
198	2.17E-08	5.00E-08	1.0E-05	.100
199	2.17E-08	5.00E-08	1.0E-05	.100
200	2.17E-08	5.00E-08	1.0E-05	.100
201	2.17E-06	5.00E-06	1.0E-05	.100
202	2.17E-06	5.00E-06	1.0E-06	.100
203	2.17E-06	5.00E-06	1.0E-06	.100
204	2.17E-06	5.00E-06	1.0E-06	.100
205	2.17E-06	5.00E-06	1.0E-05	.100
206	2.17E-05	5.00E-05	1.0E-05	.100
207	2.17E-05	5.00E-05	1.0E-05	.100
208	2.17E-05	5.00E-05	1.0E-05	.100
209	3.46E-09	7.97E-09	1.0E-04	.100
210	3.46E-09	7.97E-09	1.0E-04	.100
211	3.46E-09	7.97E-09	1.0E-04	.100
212	3.46E-09	7.97E-09	1.0E-04	.100
213	2.17E-08	5.00E-08	1.0E-05	.100
214	2.17E-08	5.00E-08	1.0E-05	.100
215	2.17E-08	5.00E-08	1.0E-05	.100
216	2.17E-08	5.00E-08	1.0E-05	.100
217	2.17E-06	5.00E-06	1.0E-05	.100
218	2.17E-06	5.00E-06	1.0E-05	.100
219	2.17E-06	5.00E-06	1.0E-05	.100
220	2.17E-06	5.00E-06	1.0E-05	.100
221	2.17E-06	5.00E-06	1.0E-05	.100
222	2.17E-05	5.00E-05	1.0E-05	.100
223	2.17E-05	5.00E-05	1.0E-05	.100
224	2.17E-05	5.00E-05	1.0E-05	.100

>?

DISPERSIVITY (m) LONGITUDINAL	TRANSVERSE
20.0	2.0

FOR ALL ELEMENTS

(INTERA, 1981)

Table 1. (cont)

ELEMENT NUMBER	HYDRAULIC (m/sec) CONDUCTIVITY (X)	(Y)	STORAGE	POROSITY
225	3.46E-09	7.97E-09	1.0E-04	.100
226	3.46E-09	7.97E-09	1.0E-04	.100
227	3.46E-09	7.97E-09	1.0E-04	.100
228	3.46E-09	7.97E-09	1.0E-04	.100
229	2.17E-08	5.00E-08	1.0E-05	.100
230	2.17E-09	5.00E-09	1.0E-05	.100
231	2.17E-09	5.00E-09	1.0E-05	.100
232	2.17E-06	5.00E-06	1.0E-05	.100
233	2.17E-06	5.00E-06	1.0E-05	.100
234	2.17E-06	5.00E-06	1.0E-05	.100
235	2.17E-06	5.00E-06	1.0E-05	.100
236	2.17E-06	5.00E-06	1.0E-05	.100
237	2.17E-06	5.00E-06	1.0E-05	.100
238	2.17E-07	5.00E-07	1.0E-05	.100
239	2.17E-06	5.00E-06	1.0E-05	.100
240	2.17E-07	5.00E-07	1.0E-05	.100
241	3.46E-09	7.97E-09	1.0E-04	.100
242	3.46E-09	7.97E-09	1.0E-04	.100
243	3.46E-09	7.97E-09	1.0E-04	.100
244	3.46E-09	7.97E-09	1.0E-04	.100
245	2.17E-09	5.00E-09	1.0E-05	.100
246	2.17E-09	5.00E-09	1.0E-05	.100
247	2.17E-09	5.00E-09	1.0E-05	.100
248	2.17E-06	5.00E-06	1.0E-05	.100
249	2.17E-06	5.00E-06	1.0E-05	.100
250	2.17E-06	5.00E-06	1.0E-05	.100
251	2.17E-06	5.00E-06	1.0E-05	.100
252	2.17E-06	5.00E-06	1.0E-05	.100
253	2.17E-06	5.00E-06	1.0E-05	.100
254	2.17E-06	5.00E-06	1.0E-05	.100
255	2.17E-06	5.00E-06	1.0E-05	.100
256	2.17E-06	5.00E-06	1.0E-05	.100

>?

DISPERSIVITY (m) LONGITUDINAL	TRANSVERSE
20.0	2.0

FOR ALL ELEMENTS

(INTERA, 1981)

Table 2. Derived Values for the Hydraulic Conductivity of the Head Distribution: Magenta Unit

ELEMENT NUMBER	HYDRAULIC CONDUCTIVITY (m/sec) (X)	(Y)	STORAGE	POROSITY
1	5.10E-05	5.10E-05	1.0E-02	.100
2	5.10E-05	5.10E-05	1.0E-02	.100
3	5.10E-05	5.10E-05	1.0E-02	.100
4	5.10E-05	5.10E-05	1.0E-02	.100
5	5.10E-05	5.10E-05	1.0E-02	.100
6	5.10E-05	5.10E-05	1.0E-02	.100
7	5.10E-05	5.10E-05	1.0E-02	.100
8	5.10E-05	5.10E-05	1.0E-02	.100
9	5.10E-05	5.10E-05	1.0E-02	.100
10	5.10E-05	5.10E-05	1.0E-02	.100
11	5.10E-05	5.10E-05	1.0E-02	.100
12	5.10E-05	5.10E-05	1.0E-02	.100
13	1.04E-05	1.04E-05	1.0E-06	.100
14	1.04E-05	1.04E-05	1.0E-06	.100
15	1.04E-05	1.04E-05	1.0E-06	.100
16	1.04E-05	1.04E-05	1.0E-06	.100
17	5.10E-05	5.10E-05	1.0E-02	.100
18	5.10E-05	5.10E-05	1.0E-02	.100
19	5.10E-05	5.10E-05	1.0E-02	.100
20	5.10E-05	5.10E-05	1.0E-02	.100
21	5.10E-05	5.10E-05	1.0E-02	.100
22	5.10E-05	5.10E-05	1.0E-02	.100
23	5.10E-05	5.10E-05	1.0E-02	.100
24	5.10E-05	5.10E-05	1.0E-02	.100
25	5.10E-05	5.10E-05	1.0E-02	.100
26	5.10E-06	5.10E-06	1.0E-02	.100
27	5.10E-06	5.10E-06	1.0E-02	.100
28	5.10E-05	5.10E-05	1.0E-02	.100
29	1.04E-05	1.04E-05	1.0E-06	.100
30	1.04E-05	1.04E-05	1.0E-06	.100
31	1.04E-05	1.04E-05	1.0E-06	.100
32	1.04E-05	1.04E-05	1.0E-06	.100
33	5.10E-05	5.10E-05	1.0E-02	.100
34	5.10E-05	5.10E-05	1.0E-06	.100
35	5.10E-05	5.10E-05	1.0E-06	.100
36	5.10E-05	5.10E-05	1.0E-06	.100
37	5.10E-05	5.10E-05	1.0E-06	.100
38	5.10E-05	5.10E-05	1.0E-06	.100
39	5.10E-05	5.10E-05	1.0E-06	.100
40	1.00E-20	1.00E-20	1.0E-06	.100
41	5.10E-06	5.10E-06	1.0E-05	.100
42	5.10E-06	5.10E-06	1.0E-02	.100
43	5.10E-06	5.10E-06	1.0E-02	.100
44	5.10E-05	5.10E-05	1.0E-02	.100
45	1.04E-05	1.04E-05	1.0E-06	.100
46	1.04E-05	1.04E-05	1.0E-06	.100
47	1.04E-05	1.04E-05	1.0E-06	.100
48	1.04E-05	1.04E-05	1.0E-06	.100
49	2.00E-06	2.00E-06	1.0E-04	.100
50	2.00E-06	2.00E-06	1.0E-04	.100
51	2.00E-06	2.00E-06	1.0E-04	.100
52	2.00E-06	2.00E-06	1.0E-04	.100
53	2.00E-06	2.00E-06	1.0E-04	.100
54	1.00E-06	1.00E-06	1.0E-04	.100
55	1.00E-06	1.00E-06	1.0E-04	.100
56	5.10E-05	5.10E-05	1.0E-02	.100

>?

DISPERSIVITY (m) LONGITUDINAL	TRANSVERSE
20.0	2.0

FOR ALL ELEMENTS

(INTERA, 1981)

Table 2. (cont)

ELEMENT NUMBER	HYDRAULIC CONDUCTIVITY (m/sec) (X)	(Y)	STORAGE	PRORSITY
57	5.10E-06	5.10E-06	1.0E-02	.100
58	5.10E-06	5.10E-06	1.0E-02	.100
59	5.10E-06	5.10E-06	1.0E-02	.100
60	5.10E-05	5.10E-05	1.0E-02	.100
61	1.04E-05	1.04E-05	1.0E-06	.100
62	1.04E-05	1.04E-05	1.0E-06	.100
63	1.04E-05	1.04E-05	1.0E-06	.100
64	1.04E-05	1.04E-05	1.0E-06	.100
65	2.00E-06	2.00E-06	1.0E-06	.100
66	2.00E-06	2.00E-06	1.0E-06	.100
67	1.00E-08	1.00E-08	1.0E-05	.100
68	1.00E-20	1.00E-20	1.0E-05	.100
69	1.00E-08	1.00E-08	1.0E-05	.100
70	1.00E-06	1.00E-06	1.0E-04	.100
71	1.00E-06	1.00E-06	1.0E-04	.100
72	5.10E-06	5.10E-06	1.0E-02	.100
73	5.10E-06	5.10E-06	1.0E-02	.100
74	5.10E-06	5.10E-06	1.0E-02	.100
75	5.10E-06	5.10E-06	1.0E-02	.100
76	5.10E-06	5.10E-06	1.0E-02	.100
77	1.04E-06	1.04E-06	1.0E-06	.100
78	1.04E-06	1.04E-06	1.0E-06	.100
79	1.04E-06	1.04E-06	1.0E-06	.100
80	1.04E-06	1.04E-06	1.0E-06	.100
81	3.00E-07	3.00E-07	1.0E-09	.100
82	3.00E-07	3.00E-07	1.0E-09	.100
83	3.00E-07	3.00E-07	1.0E-09	.100
84	3.00E-07	3.00E-07	1.0E-09	.100
85	3.00E-07	3.00E-07	1.0E-06	.100
86	8.46E-09	8.46E-09	1.0E-06	.100
87	8.46E-09	8.46E-09	1.0E-06	.100
88	1.85E-07	1.85E-07	1.0E-05	.100
89	5.00E-07	5.00E-07	1.0E-05	.100
90	5.00E-07	5.00E-07	1.0E-05	.100
91	5.00E-07	5.00E-07	1.0E-05	.100
92	1.85E-07	1.85E-07	1.0E-05	.100
93	0.33E-07	0.33E-07	1.0E-05	.100
94	0.33E-07	0.33E-07	1.0E-05	.100
95	0.33E-07	0.33E-07	1.0E-05	.100
96	0.33E-07	0.33E-07	1.0E-05	.100
97	1.14E-07	1.14E-07	1.0E-09	.100
98	1.14E-07	1.14E-07	1.0E-09	.100
99	1.14E-07	1.14E-07	1.0E-09	.100
100	1.14E-07	1.14E-07	1.0E-09	.100
101	1.69E-09	1.69E-09	1.0E-06	.100
102	2.00E-09	2.00E-09	1.0E-06	.100
103	2.00E-09	2.00E-09	1.0E-06	.100
104	1.00E-08	1.00E-08	1.0E-07	.100
105	1.00E-08	1.00E-08	1.0E-07	.100
106	5.00E-08	5.00E-08	1.0E-05	.100
107	3.30E-07	3.30E-07	1.0E-07	.100
108	0.33E-06	0.33E-06	1.0E-07	.100
109	0.33E-06	0.33E-06	1.0E-07	.100
110	0.33E-06	0.33E-06	1.0E-07	.100
111	0.33E-06	0.33E-06	1.0E-07	.100
112	0.33E-06	0.33E-06	1.0E-07	.100

>?

DISPERSIVITY (m) LONGITUDINAL	TRANSVERSE
20.0	2.0

FOR ALL ELEMENTS

(INTERA, 1981)

Table 2. (cont)

ELEMENT NUMBER	HYDRAULIC CONDUCTIVITY (m/sec) (X)	(Y)	STORAGE	POROSITY
113	1.14E-07	1.14E-07	1.0E-09	.100
114	1.14E-07	1.14E-07	1.0E-09	.100
115	1.14E-07	1.14E-07	1.0E-09	.100
116	1.14E-07	1.14E-07	1.0E-09	.100
117	8.45E-09	8.45E-09	1.0E-05	.100
118	8.45E-09	8.45E-09	1.0E-06	.100
119	8.45E-09	8.45E-09	1.0E-06	.100
120	5.00E-08	5.00E-08	1.0E-04	.100
121	5.00E-08	5.00E-08	1.0E-04	.100
122	3.00E-05	3.00E-05	1.0E-05	.100
123	1.00E-05	1.00E-05	1.0E-05	.100
124	1.00E-05	1.00E-05	1.0E-05	.100
125	1.00E-06	1.00E-06	1.0E-05	.100
126	1.00E-06	1.00E-06	1.0E-05	.100
127	1.00E-06	1.00E-06	1.0E-05	.100
128	1.00E-06	1.00E-06	1.0E-05	.100
129	4.50E-07	4.50E-07	1.0E-09	.100
130	4.50E-07	4.50E-07	1.0E-09	.100
131	1.70E-06	1.70E-06	1.0E-09	.100
132	1.70E-06	1.70E-06	1.0E-09	.100
133	2.55E-08	2.55E-08	1.0E-06	.100
134	2.55E-08	2.55E-08	1.0E-06	.100
135	1.40E-08	1.40E-08	1.0E-05	.100
136	2.80E-09	2.80E-09	1.0E-05	.100
137	4.00E-09	4.00E-09	1.0E-04	.100
138	1.00E-07	1.00E-07	1.0E-05	.100
139	1.00E-07	1.00E-07	1.0E-05	.100
140	1.00E-07	1.00E-07	1.0E-05	.100
141	1.40E-07	1.40E-07	1.0E-05	.100
142	1.40E-07	1.40E-07	1.0E-05	.100
143	1.40E-07	1.40E-07	1.0E-05	.100
144	1.40E-07	1.40E-07	1.0E-05	.100
145	3.40E-07	3.40E-07	1.0E-09	.100
146	3.40E-07	3.40E-07	1.0E-09	.100
147	1.70E-06	1.70E-06	1.0E-09	.100
148	1.70E-06	1.70E-06	1.0E-09	.100
149	1.27E-06	1.27E-06	1.0E-06	.100
150	1.27E-06	1.27E-06	1.0E-06	.100
151	7.05E-08	7.05E-08	1.0E-05	.100
152	1.41E-08	1.41E-08	1.0E-05	.100
153	1.31E-08	1.31E-08	1.0E-05	.100
154	2.62E-08	2.62E-08	1.0E-05	.100
155	1.31E-07	1.31E-07	1.0E-05	.100
156	1.31E-07	1.31E-07	1.0E-05	.100
157	1.40E-07	1.40E-07	1.0E-05	.100
158	1.40E-07	1.40E-07	1.0E-05	.100
159	1.40E-07	1.40E-07	1.0E-05	.100
160	1.40E-07	1.40E-07	1.0E-05	.100
161	3.40E-07	3.40E-07	1.0E-09	.100
162	3.40E-07	3.40E-07	1.0E-09	.100
163	1.70E-06	1.70E-06	1.0E-09	.100
164	1.70E-06	1.70E-06	1.0E-09	.100
165	1.65E-07	1.65E-07	1.0E-05	.100
166	1.65E-07	1.65E-07	1.0E-05	.100
167	5.00E-07	5.00E-07	1.0E-05	.100
168	5.00E-07	5.00E-07	1.0E-05	.100

>?

DISPERSIVITY (m) LONGITUDINAL	TRANSVERSE
20.0	2.0

FOR ALL ELEMENTS

(INTERA, 1981)

Table 2. (cont)

ELEMENT NUMBER	HYDRAULIC CONDUCTIVITY (m/sec) (X)	(Y)	STORAGE	POROSITY
169	1.31E-08	1.31E-08	1.0E-05	.100
170	1.31E-08	1.31E-08	1.0E-05	.100
171	1.31E-08	1.31E-08	1.0E-05	.100
172	1.31E-07	1.31E-07	1.0E-05	.100
173	1.40E-07	1.40E-07	1.0E-05	.100
174	1.40E-07	1.40E-07	1.0E-05	.100
175	1.40E-07	1.40E-07	1.0E-05	.100
176	1.40E-07	1.40E-07	1.0E-05	.100
177	1.47E-07	1.47E-07	1.0E-03	.100
178	1.47E-07	1.47E-07	1.0E-03	.100
179	7.35E-07	7.35E-07	1.0E-03	.100
180	7.35E-07	7.35E-07	1.0E-03	.100
181	7.35E-07	7.35E-07	1.0E-03	.100
182	5.00E-06	5.00E-06	1.0E-05	.100
183	5.00E-06	5.00E-06	1.0E-05	.100
184	5.00E-06	5.00E-06	1.0E-05	.100
185	1.31E-08	1.31E-08	1.0E-05	.100
186	1.31E-08	1.31E-08	1.0E-05	.100
187	1.30E-08	1.30E-08	1.0E-05	.100
188	1.31E-07	1.31E-07	1.0E-05	.100
189	1.40E-07	1.40E-07	1.0E-05	.100
190	1.40E-07	1.40E-07	1.0E-05	.100
191	1.40E-07	1.40E-07	1.0E-05	.100
192	1.40E-07	1.40E-07	1.0E-05	.100
193	1.47E-08	1.47E-08	1.0E-05	.100
194	1.47E-08	1.47E-08	1.0E-05	.100
195	7.35E-08	7.35E-08	1.0E-05	.100
196	7.35E-08	7.35E-08	1.0E-05	.100
197	7.35E-06	7.35E-06	1.0E-05	.100
198	5.00E-06	5.00E-06	1.0E-05	.100
199	5.00E-06	5.00E-06	1.0E-05	.100
200	5.00E-06	5.00E-06	1.0E-05	.100
201	1.31E-08	1.31E-08	1.0E-05	.100
202	1.31E-08	1.31E-08	1.0E-05	.100
203	1.31E-08	1.31E-08	1.0E-05	.100
204	1.31E-07	1.31E-07	1.0E-05	.100
205	1.40E-07	1.40E-07	1.0E-05	.100
206	1.40E-07	1.40E-07	1.0E-05	.100
207	1.40E-07	1.40E-07	1.0E-05	.100
208	1.40E-07	1.40E-07	1.0E-05	.100
209	1.47E-08	1.47E-08	1.0E-03	.100
210	1.47E-08	1.47E-08	1.0E-03	.100
211	1.47E-08	1.47E-08	1.0E-03	.100
212	1.47E-08	1.47E-08	1.0E-03	.100
213	1.47E-07	1.47E-07	1.0E-03	.100
214	1.00E-07	1.00E-07	1.0E-05	.100
215	1.00E-07	1.00E-07	1.0E-05	.100
216	1.00E-07	1.00E-07	1.0E-05	.100
217	1.00E-07	1.00E-07	1.0E-05	.100
218	1.00E-07	1.00E-07	1.0E-05	.100
219	1.00E-07	1.00E-07	1.0E-05	.100
220	1.00E-07	1.00E-07	1.0E-05	.100
221	1.40E-06	1.40E-06	1.0E-05	.100
222	1.40E-06	1.40E-06	1.0E-05	.100
223	1.40E-06	1.40E-06	1.0E-05	.100
224	1.40E-06	1.40E-06	1.0E-05	.100

>?

DISPERSIVITY (m)

LONGITUDINAL	TRANSVERSE
20.0	2.0

FOR ALL ELEMENTS

(INTERA, 1981)

Table 2. (cont)

ELEMENT NUMBER	HYDRAULIC (m/sec) CONDUCTIVITY (X)	(Y)	STORAGE	POROSITY
225	1.47E-08	1.47E-08	1.0E-03	.100
226	1.47E-08	1.47E-08	1.0E-03	.100
227	1.47E-08	1.47E-08	1.0E-03	.100
228	1.47E-08	1.47E-08	1.0E-03	.100
229	1.47E-07	1.47E-07	1.0E-03	.100
230	1.00E-07	1.00E-07	1.0E-05	.100
231	1.00E-07	1.00E-07	1.0E-05	.100
232	1.00E-07	1.00E-07	1.0E-05	.100
233	1.00E-07	1.00E-07	1.0E-05	.100
234	1.00E-07	1.00E-07	1.0E-05	.100
235	1.00E-07	1.00E-07	1.0E-05	.100
236	1.00E-07	1.00E-07	1.0E-05	.100
237	1.40E-06	1.40E-06	1.0E-05	.100
238	1.40E-06	1.40E-06	1.0E-05	.100
239	1.40E-06	1.40E-06	1.0E-05	.100
240	1.40E-06	1.40E-06	1.0E-05	.100
241	1.47E-08	1.47E-08	1.0E-03	.100
242	1.47E-08	1.47E-08	1.0E-03	.100
243	1.47E-08	1.47E-08	1.0E-03	.100
244	1.47E-07	1.47E-07	1.0E-03	.100
245	1.47E-07	1.47E-07	1.0E-03	.100
246	1.00E-07	1.00E-07	1.0E-05	.100
247	1.00E-07	1.00E-07	1.0E-05	.100
248	1.00E-07	1.00E-07	1.0E-05	.100
249	1.00E-07	1.00E-07	1.0E-05	.100
250	1.00E-07	1.00E-07	1.0E-05	.100
251	1.00E-07	1.00E-07	1.0E-05	.100
252	1.00E-07	1.00E-07	1.0E-05	.100
253	1.40E-07	1.40E-07	1.0E-05	.100
254	1.40E-07	1.40E-07	1.0E-05	.100
255	1.40E-07	1.40E-07	1.0E-05	.100
256	1.40E-07	1.40E-07	1.0E-05	.100

>?

DISPERSIVITY (m) LONGITUDINAL	TRANSVERSE
20.0	2.0

FOR ALL ELEMENTS

(INTERA, 1981)

By way of crude example, if it is presumed that WIPP accepts 10^6 drums of TRU rubbish with an average loading of 1 g of Pu, then the repository inventory is 10^6 g of Pu. If it is assumed that this inventory is released over 10^3 yr, the flow in the Culebra over the site (2×10^2 m^3/yr) implies a concentration of ~5 ppm. For a very acidic fluid (pH ~3), the solubility limit for any state of Pu is ~20 ppm (D. Rai et al, 1980). Actual fluid pHs are measured in the Culebra in the range of 6 to 9, where the solubility limit is at least two orders of magnitude smaller and limits the maximum concentration in the Culebra by at least the same factor. Thus the unit source could be interpreted as 0.02 to 0.2 ppm and the time for exhaustion of the inventory 2.5×10^4 to 2.5×10^5 yr, ignoring radioactive decay.

The Magenta and Culebra Dolomite Aquifers

These two fluid-bearing units of the Rustler Formation are of differing importance in transport considerations and generally seem to be hydraulically distinct (Gonzalez, 1983b) (except perhaps in Nash Draw) and are discussed here separately. Two basic results are extracted for each unit from these separate calculations: (a) the self-consistent distribution of potentiometric heads on a regional scale (16 × 16 mi, 25.8 × 25.8 km); and (b) the movement of contaminants introduced continously into each unit. The stratigraphic positions of the Magenta and Culebra Dolomites are shown in Figure 2 (Gonzalez, 1983a). The Culebra is discussed first, since it appears to be more important.

Culebra Unit

The data for the Culebra for the 16 mi × 16 mi region being modeled consist of water level measurements, pump tests, and slug tests at 19 different locations. The measured wells that were used were H-1 through H-10, USGS-1, P-14, P-15, P-17, P-18, W-25 through W-28, and W-30. The measurements and modes of testing are described by Gonzalez (1983a), except for USGS-1, described by Cooper et al (1971). The physical characteristics of the unit and its inferred hydraulic properties are discussed in Cooper et al (1971) and Gonzalez (1983a). The need to determine if the medium was isotropic led to the selection of three sites that were examined at length by Hydro Geo Chem, Inc and by D. Gonzalez, SNL (Ward et al, 1983). The tests for anisotropy at three locations, H-4, H-5, and H-6, show that the Culebra is anisotropic with the ratio of major-to-minor axis values for the transmissivity in the range of 1:2.3 to 1:2.7, with the major axis oriented roughly NW-SE. This analysis, which is rather involved, is discussed in detail in Ward et al (1983). As a result, anisotropy assignment of hydraulic conductivity to all 256 elements in this study region was aligned insofar as possible with the principal axes of transmissivity and the ratio of the x and y components of hydraulic conductivity was maintained at 1:2.3. (Other values of this ratio were investigated, with little difference on this scale.) The initial assignment of these values is shown in Figure 3 for the regions ascribed to the wells. Other values were assigned on the basis of surrounding data and the regional trend.

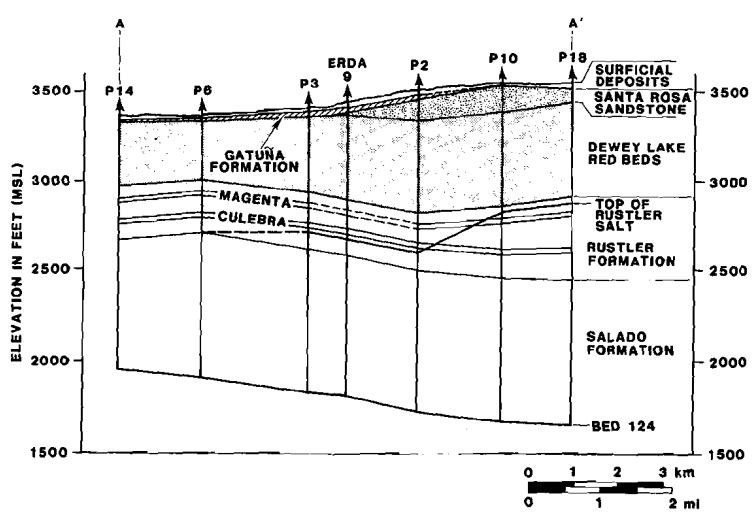

Figure 2. Geologic Section Across the WIPP Site

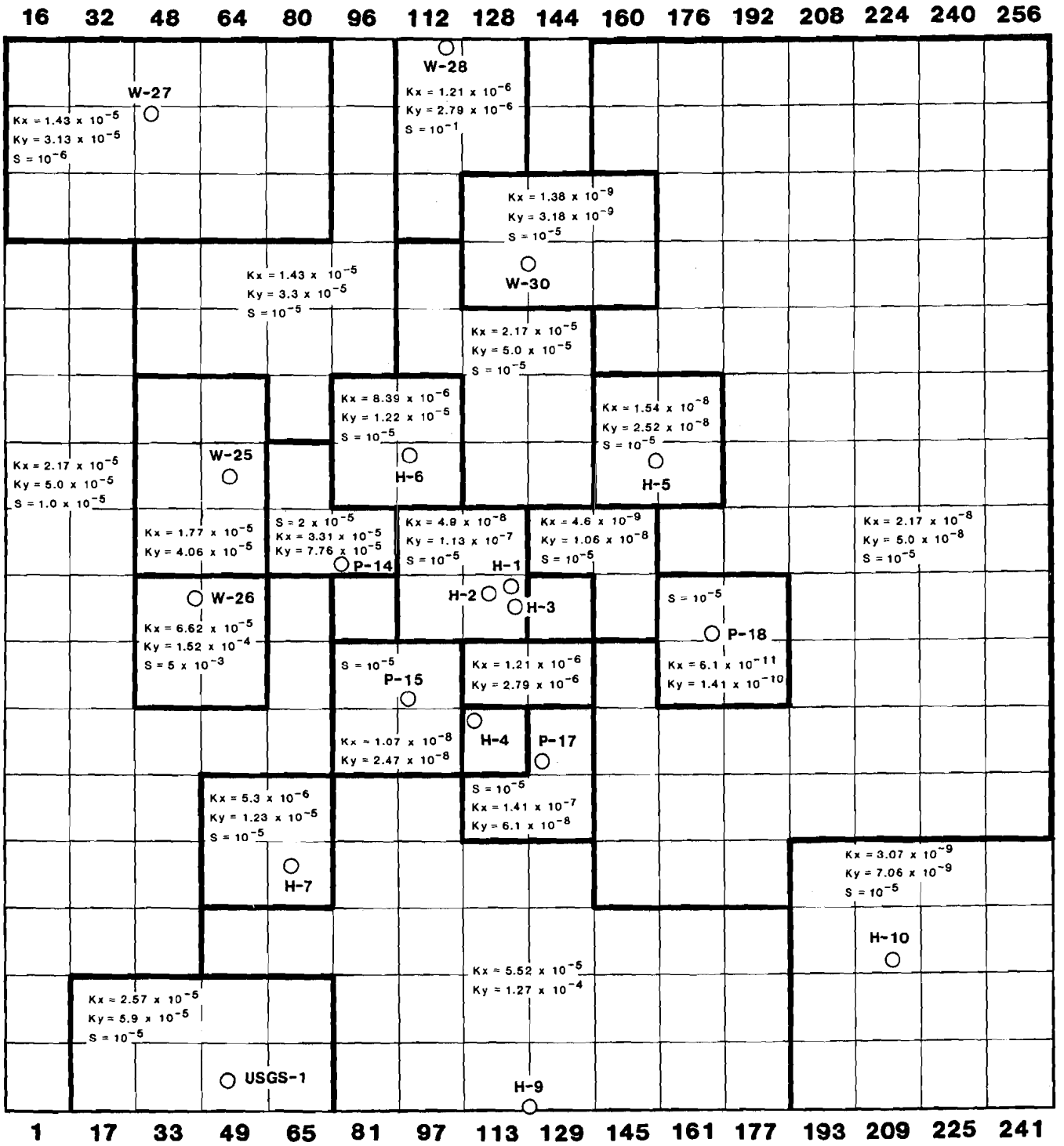

Figure 3. Areal Assignment of Initial Hydraulic conductivity – K (m/s), and Storativity – s, in the x and y Directions Relative to the Major Transmissivity Tensor for the Culebra Dolomite. The WIPP site is located at the center of the finite-element grid. The numbers, top and bottom, are element numbers for adjacent elements.

The initial calculated distribution of head potentials is shown in Figure 4. The distribution is somewhat irregular, particularly southeast of the site, which is indicated in this figure by an eight-sided figure at the center of the grid system. The location of the potentiometric contours, while relatively insensitive on this scale to change in hydraulic properties, is sensitive to the values fixed at the well points. Areas to the north, near W-30, H-5, AEC-7, and AEC-8, and to the southwest of the site have few available head data. Data are numerous close to the site. Figure 4 also suggests several closed contours. These result from the presence of single wells near these locations, and from the imposed requirement that head potentials at these wells remained fixed. This head distribution forms the basis for deriving the self-consistent head distribution, shown in Figure 5, which exhibits a more regular steady-state head distribution with the same general structure as shown in Figure 4. This is especially true in the immediate vicinity of the site, where the data coverage is more complete. Corresponding derived values for the hydraulic conductivity are listed in Table 1. The match to the field measurements of head is reasonably good except at W-30, which is either low or is part of a pattern draining to the N-E, where there are no data, and at W-26, where no further effort was made to make a better match because of its position relative to the rest of the flow. The head at Well P-18 is an uncertain datum because of measurement problems and a very slow recovery; no comparison is shown there (Mercer, personal communication).

The modeling of the contaminant plume was begun by assuming a continuous input of contamination at a concentration of one unit at the center of the grid. The initial configuration within a 2.4 × 2.4 km (1.5 × 1.5 mi) block is shown in Figure 6. An initial contaminant plume is assume to exist at time zero. It is further assumed that local hydraulic properties and head distribution are unchanged by contaminant injection; the only effect is a local concentration "mounding" of contaminant.

The motion and growth of this plume is followed through Figure 7 at 21 yr and through Figure 8 at 42 yr. After this time, 42 yr, the plume front (taken to be 10^{-3} of source) is interacting with the boundary and the concentration data are then transferred to the next larger cutout 4.8 × 4.8 km (3 × 3 mi). This and the next two levels of the problem have an additional 78 interior nodes at the center of the grid so that a minimum of data is lost due to the change in scale in the transfer. The plume is followed for 130 yr on this scale and then transferred to the next larger scale 9.68 × 9.68 km (6 × 6 mi) in the same manner. After an additional 130 yr the plume is transferred to the large-scale grid 25.8 × 25.8 km (16 × 16 mi) and the calculations continued. The transfer in this case was made long before there was any important interaction with the boundary. The two intervening plumes for intermediate scales are not shown. The start of the plume in the large scale, Figure 9, is 302 yr after the plume was initiated. Heads are less regular on this scale than on the previous scales; this shows up in somewhat erratic movement of the plume. At 468.9 yr (Figure 10) the plume has moved downgradient to the southeast, with some spread due to numerical diffusion to the northwest. At 553 yr (Figure 11) the plume is beginning to see the steeper gradients and high hydraulic conductivity to the west and, as seen in the succeeding figure (Figure 12), spreads downgradient by 638.4 yr. However, by 808 yr (Figure 13) the spread west has slowed in a region of low gradient. At this time, on the scale shown, the plume has essentially become static; Figure 14 shows the position some 600 yr later (at 1405 yr). The average velocities over their 1400-yr period have been 3.5 m/yr to the south and 3 m/yr to the southwest. The calculations were halted at this time because the plume had generally moved into regions of low gradient. It has practically ceased to move, becoming essentially static on this scale. While the plume front, taken to be a concentration level of 10^{-3}, effectively stops on this scale, there is still movement of contaminants through the front. Contaminants have simply been diluted below this level of concentration by aquifer fluids as they are transported. The plume front is a conservative estimate of transport since numerical dispersion and transients due to transfer to large scales produce apparent motion at least the order of one element. This also occurs upstream, giving the impression of movement against the gradient. Separate calculations of particle travel times, discussed in Appendix B, are further evidence of the effects of numerical dispersion and show even slower velocities. Previous calculations of particle travel times for Rustler fluids, contained in the FEIS (FEIS, 1980), resulted in estimated travel times of the order of 3500 yr for movement from the center of the WIPP site to Malaga Bend on the Pecos River 38 km (24 m) distant. The present calculations indicate particle travel times of the order of 130,000 yr for a much shorter distance (12.9 km (8 mi)) from the center of the site. However, particle travel times may be irrelevant to the issue of safety in certain hydraulic conditions; for example, where dilution by aquifer fluids is significant. The important travel time is that for arrival of a concentration level of each radionuclide deemed threatening.

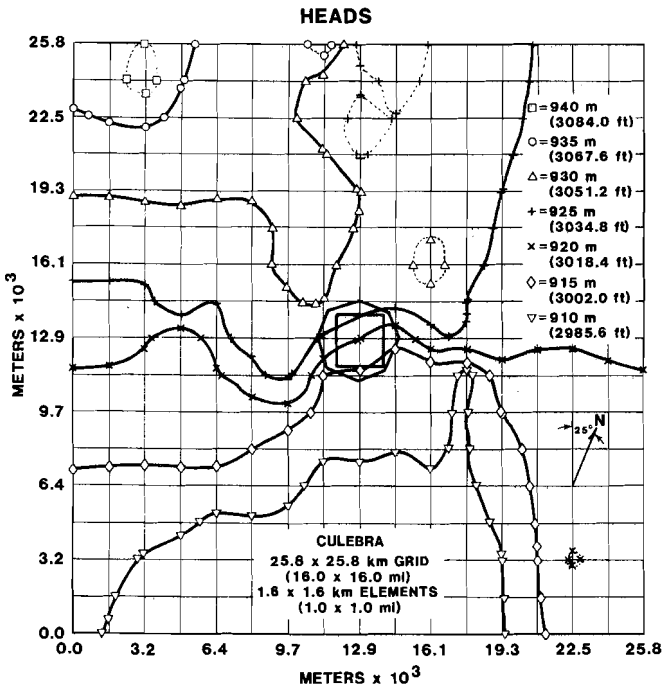

Figure 4. Head Distributions for the Culebra Dolomite, Generated With ISOQUAD, Using Assigned Boundary Conditions and Fixed Values at Wells (Closed contours resulting from constraining potentiometric surface to pass exactly through data from each well are shown by dashed lines.)

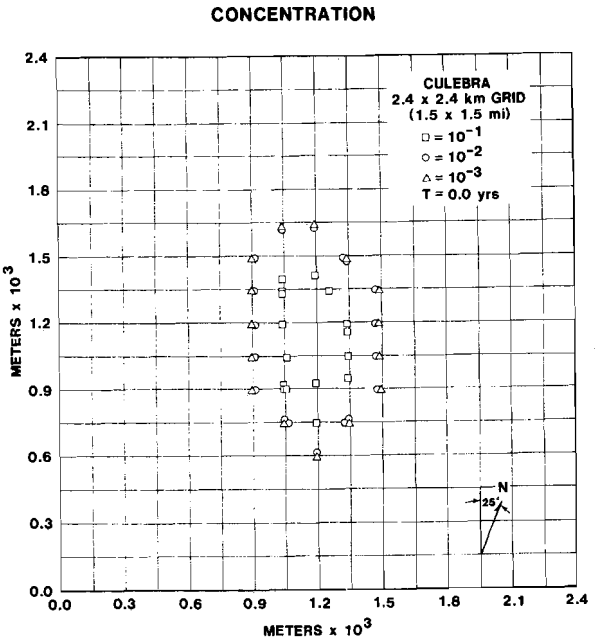

Figure 6. Initial Plume Configuration in the Culebra Dolomite at Relative Time Zero (time of discovery). Block grid is 2.5 × 2.5 km.

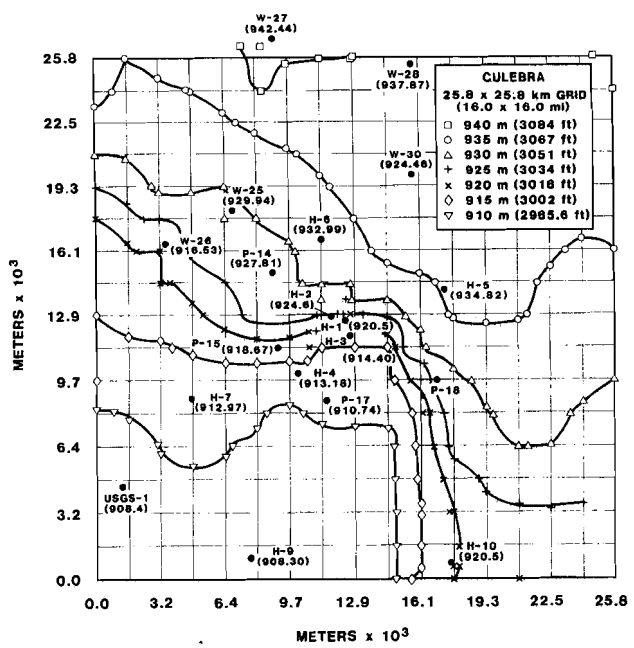

Figure 5. Derived Head Distribution for the Culebra, for the Self-Consistent Problem, With Fixed Boundaries and Varied Assignments of Hydraulic Conductivities

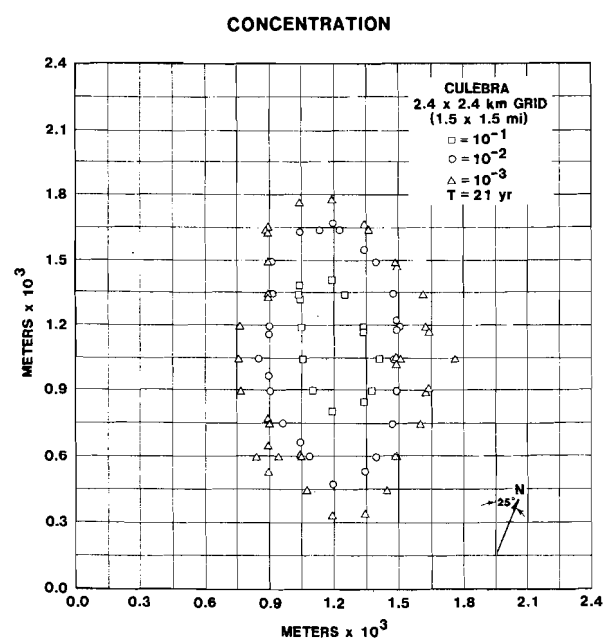

Figure 7. Plume Migration in the Culebra Dolomite for a Continuous Source Injection of One Unit at the Center of the Site. Concentration points are relative to the unit source, at 21 yr after discovery. Block grid is 2.5 × 2.5 km.

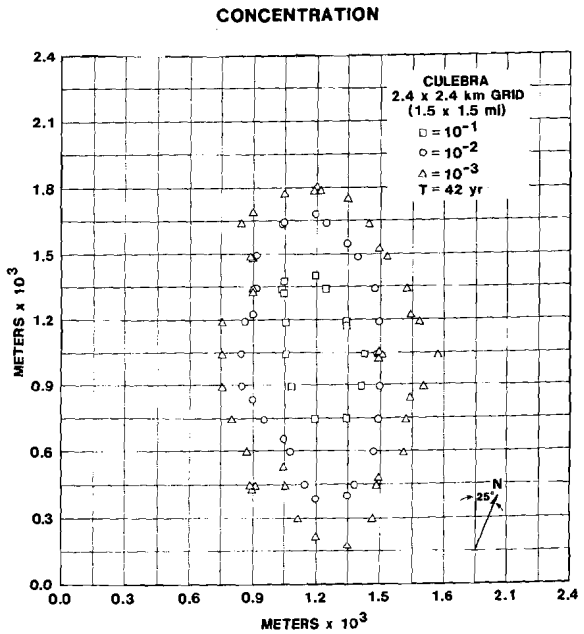

Figure 8. Plume Migration in the Culebra Dolomite for a Continuous Source Injection of One Unit at the Center of the Site. Concentration points are relative to the unit source, at 42 yr after discovery. Block grid is 2.5 × 2.5 km.

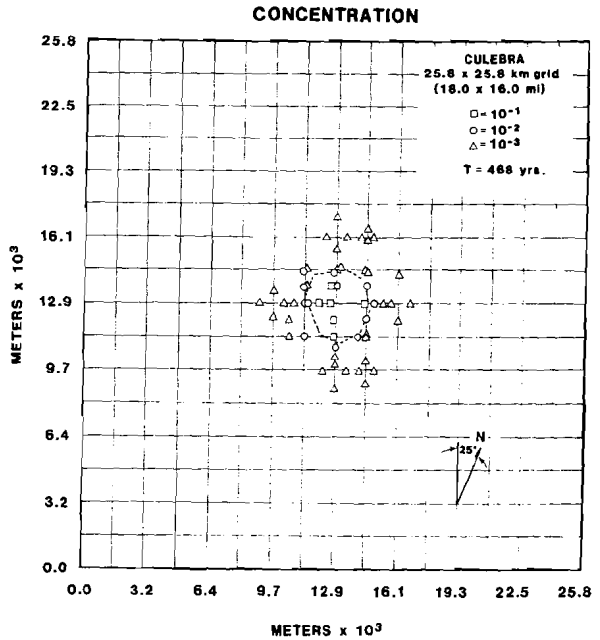

Figure 10. Plume Migration in the Culebra Dolomite for a Continuous Source Injection of One Unit at the Center of the Site. Concentration points are relative to the unit source, at 468 yr after discovery. Block grid is 2.5 × 2.5 km.

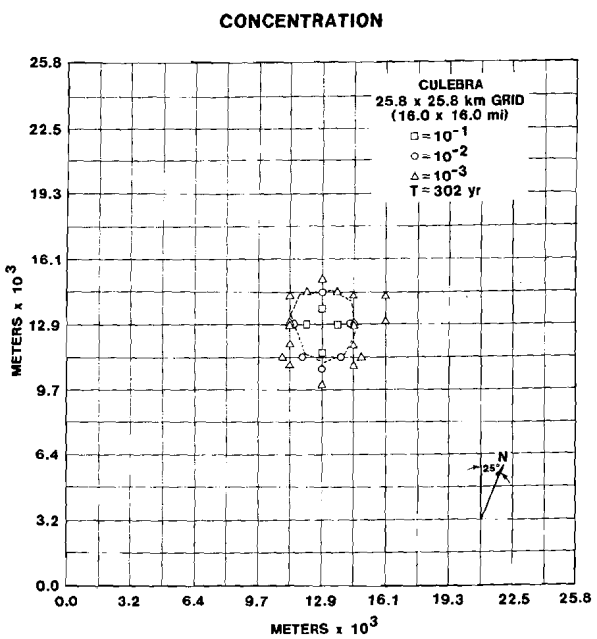

Figure 9. Plume Migration in the Culebra Dolomite for a Continuous Source Injection of One Unit at the Center of the Site. Concentration points are relative to the unit source, at 302 yr after discovery. Block grid is 2.5 × 2.5 km.

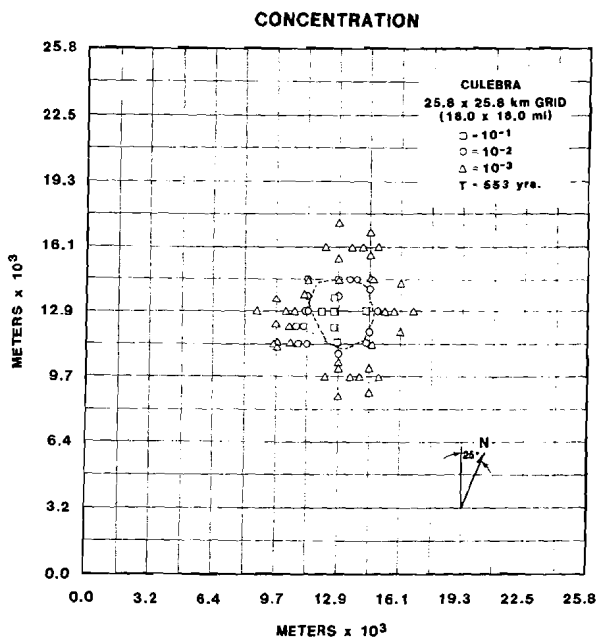

Figure 11. Plume Migration in the Culebra Dolomite for a Continuous Source Injection of One Unit at the Center of the Site. Concentration points are relative to the unit source, at 553 yr after discovery. Block grid is 2.5 × 2.5 km.

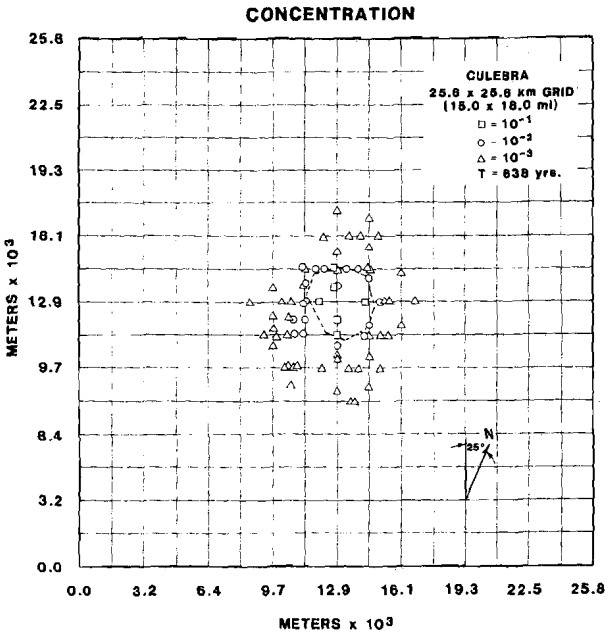

Figure 12. Plume Migration in the Culebra Dolomite for a Continuous Source Injection of One Unit at the Center of the Site. Concentration points are relative to the unit source, at 638 yr after discovery. Block grid is 2.5 × 2.5 km.

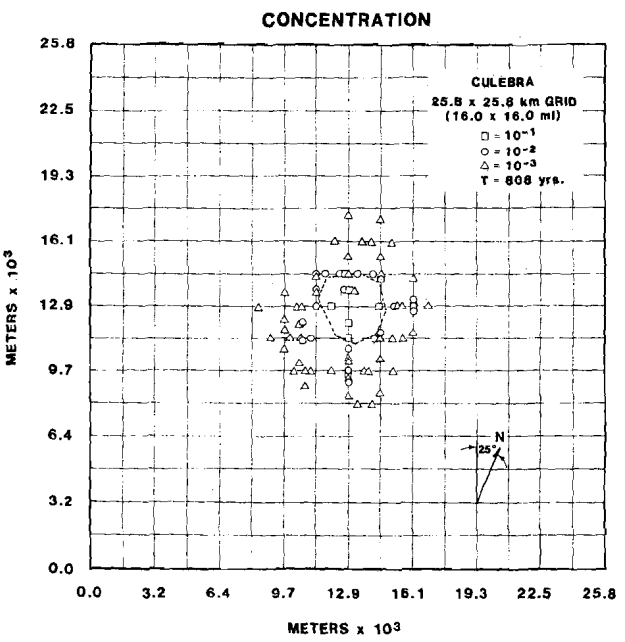

Figure 13. Plume Migration in the Culebra Dolomite for a Continuous Source Injection of One Unit at the Center of the Site. Concentration points are relative to the unit source, at 808 yr after discovery. Block grid is 2.5 × 2.5 km.

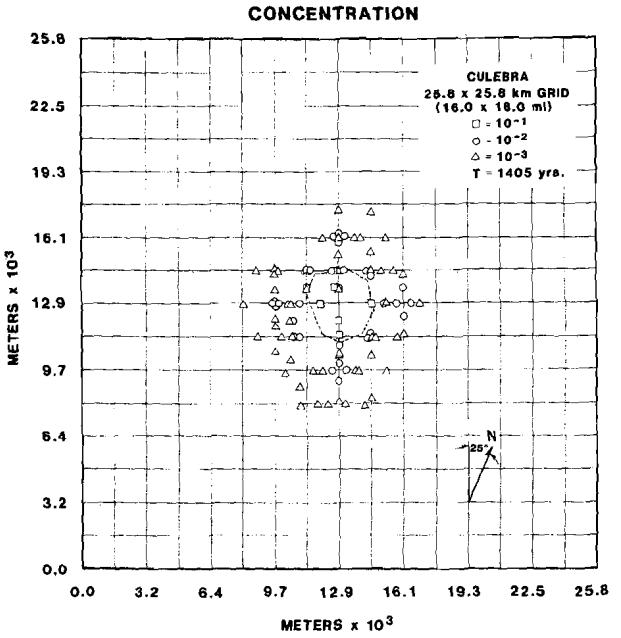

Figure 14. Plume Migration in the Culebra Dolomite for a Continuous Source Injection of One Unit at the Center of the Site. Concentration points are relative to the unit source, at 1405 yr after discovery. Block grid is 2.5 × 2.5 km.

Magenta Unit

The data for the Magenta for the 16 mi × 16 mi region modeled consist of water level measurements, slug tests, and pumptests at 10 different locations. The wells measured were H-1, H-2, H-3, H-4, H-5, H-6, H-9, H-10, W-25 and W-27. In addition there are two holes, W-26 and W-28, where the Magenta did not yield water to a well. At W-29 the Magenta Unit is not present due to erosion. The Magenta Unit is similar in character to the Culebra and is discussed by Gonzalez (1983a). This unit was not tested for anisotropy and so is presumed for the purposes here to be isotropic, although transport is so slight that this presumption is essentially irrelevant. Values for the hydraulic conductivity are assigned as shown in Figure 15, except for W-26 and W-28, which were dry and were given an extremely small value of conductivity. The initial head distribution calculated with a reflecting boundary and fixed well head values is shown in Figure 16. The corresponding self-consistent head distribution or potentiometric surface derived in these calculations is shown in Figure 17, and the corresponding derived values for the hydraulic conductivity are listed in Table 2. The head potential exhibits the steepest gradients in the vicinity of Nash Draw, to the west of the site. The repository site is indicated by the 8-sided figure (Figure 16). The smaller square inside this figure is a cutout used for a plume calculation in the

manner of that discussed for the Culebra with the same concentration input. The cutout is a 2.4 × 2.4 km (1.5 × 1.5 mi) block with 289, 150 × 150 m (492 × 492 ft) elements. A plume is assumed to have formed around a central continuous source of contaminant. The initial plume is shown in Figure 18. The extent of the plume 676 yr later is shown in Figure 19, amounting to less than 300 m (1000 ft) growth in that period (0.44 m/yr). There is so little movement in this long period, and much of that movement appears to be numerical dispersion, that it seems pointless to transfer the plume to subsequent cutouts as was done for the Culebra. To check this conclusion, we assigned to the large-size problem, 25.8 × 25.8 km (16 × 16 mi), so that the plume clearly overlapped the region of highest gradients. The results were similar; in effect, no movement on the 1610 × 1610 m (1 × 1 mi) grid scale of the calculations. This calculation is not shown. Unless the well data change substantially, or new data are added, it seems inappropriate to examine the Magenta Unit further.

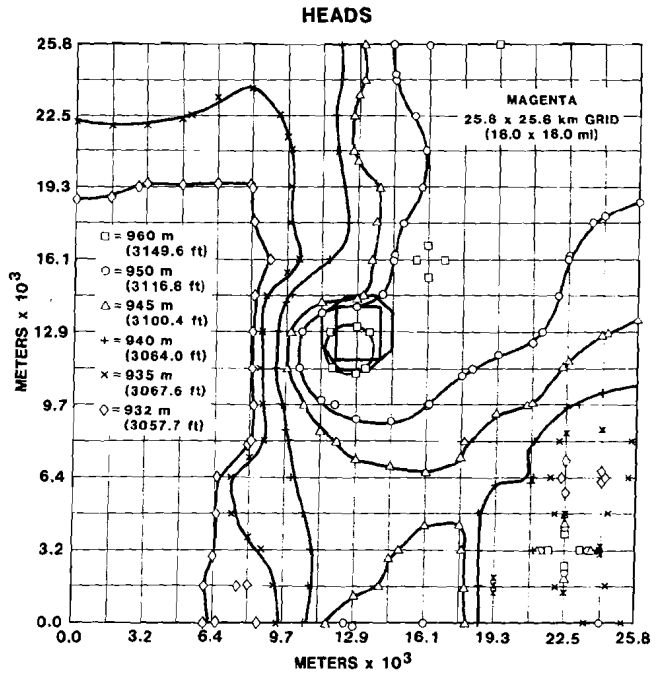

Figure 16. Initial Head Distributions for the Magenta Dolomite, Generated With ISOQUAD, Using Assigned Boundary Conditions and Fixed Values at Wells

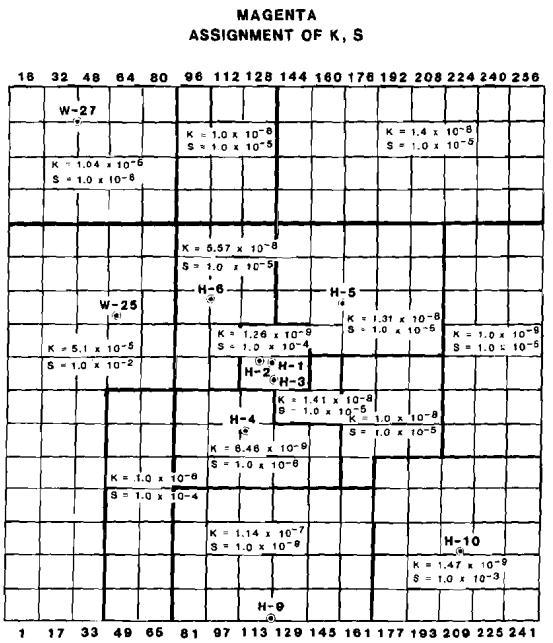

Figure 15. Areal Assignment of Initial Hydraulic Conductivity – K (m/s), and Storativity – s, in the x and y Direction Relative to the Major Transmissivity Tensor for the Magenta Dolomite. The WIPP site is located at the center of the finite-element grid. The numbers, upper and lower, are element numbers.

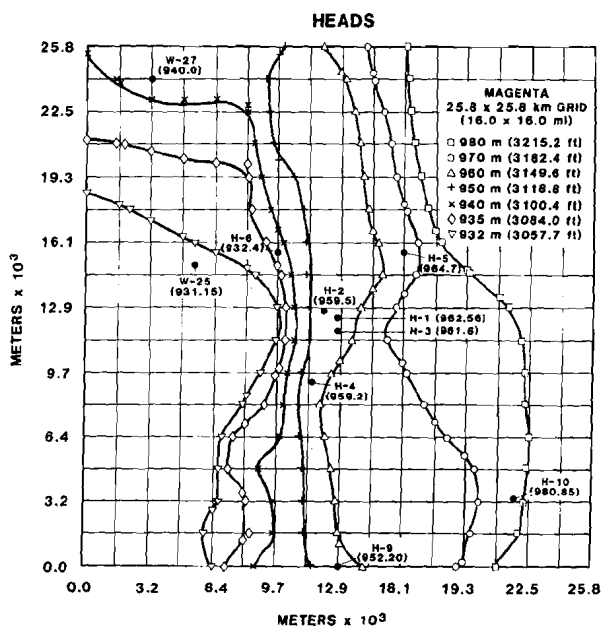

Figure 17. Derived Head Distribution for the Magenta Dolomite for the Self-Consistent Problem, With Fixed Boundaries, and Varied Assignments of Hydraulic Conductivity

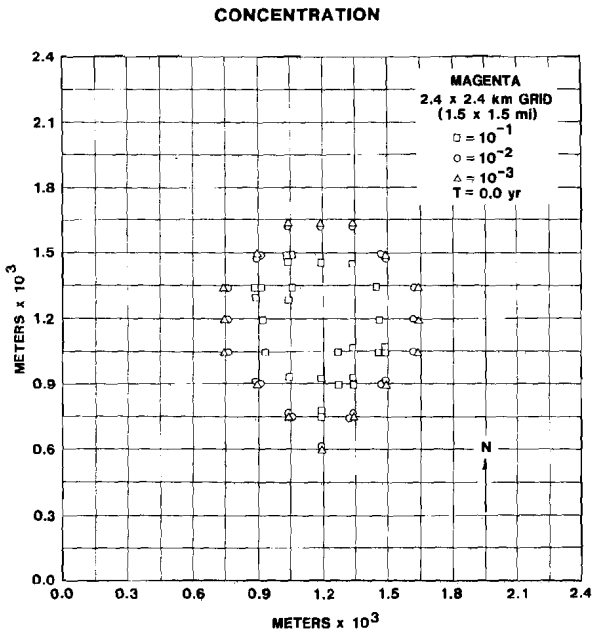

Figure 18. Initial Plume Configuration in the Magenta Dolomite at Relative Time Zero (time of discovery). Block grid is 2.5 × 2.5 km.

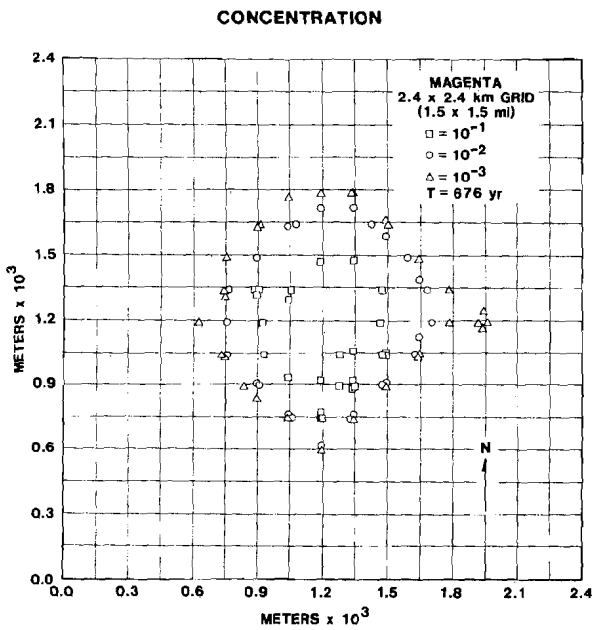

Figure 19. Plume Migration in the Culebra Dolomite for a Continuous Source Injection of One Unit at the Center of the Site. Concentration points are relative to the unit source, at 676 yr after discovery. Block grid is 2.5 × 2.5 km.

Summary

Several specific conclusions were reached as a result of this study:

1. Migration of a nonsorbing contaminant plume in the Culebra or Magenta was modeled to determine the qualitative and semiquantitative behavior of such motion. Average calculated front velocities are low (~3.5 m/yr for the Culebra) and are overestimates of the actual velocities, due to numerical dispersion and scale factors. The behavior of given concentration levels and their eventual near-halt after or before 1400 yr are shown. This result calls into question the utility of regulations based on particle or water travel times.
2. Particle travel times calculated from the particle velocities at nodes along selected streamlines from the repository are long (>1000 yr) to reach the boundary of Zone III, 2 mi from the center of the site (see FEIS, 1980), and >130,000 yr to travel 8 mi south of the site (see Appendix B).
3. Experimental drawdown and recovery curves were, with few exceptions, reasonably well-matched by the theoretical curves derived on the basis of a well in a porous medium (see Appendix A).
4. Fluid sources do not appear in the analyses of the drawdown and recovery curves (see Appendix A).

This report is preliminary, but, on the basis of the data currently available, justifies the present use of porous-medium theory in the description of flow in the filled-fracture media that constitute the Magenta and Culebra Dolomites. More hydrogeologic data will be forthcoming. When incorporated into additional modeling, these data will help broaden the basis on which porous-medium flow or other representations will better describe the hydraulic behavior of the systems.

APPENDIX A

Analyses of Supporting Data

The choice of the mathematical representation of flow by a model dependent on flow through porous media, through fractures, or through some combination of the two, depends on the analysis of field data. A porous-medium was initially chosen here, on the basis of examination of core from the Rustler Dolomites and on field interpretation of aquifer pump tests. The general characteristics of core from the Magenta and Culebra are discussed by Gonzalez (1983a).

Well tests used here are of two basic types, multi-well tracer tests (convergent flow tests, recirculating flow tests) and single-well tests (pump tests, slug tests, observation wells). Since individual well tests may allow several interpretations of the behavior of the medium, there is nonuniqueness; in fact, tests in some fractured systems mimic results in porous media (Long et al, 1982; Rushton and Redshaw, 1979). Therefore, it is necessary to look for systematics in well performances. One asks whether or not "barriers" to the flow exist and what distances and directions they are from the pumped well. Barriers to flow are for convenience defined here to be regions where the hydraulic conductivity changes or possibly where there are flow channels (sources or sinks).

In the Magenta and Culebra Dolomites, since both units are saturated, confined, and separate, any flow channels are saturated. Assessment of how far away any barriers are or how far the barrier would have to be is possible because each well that is tested by pumping interrogates a region a substantial distance out into the rock around the well. Analyses of the pump tests give a rough idea of whether the representative elementary volume of rock being sampled is of a size represented in the model and whether the choice of representation is correct. Multiple-well tests allow direct calculation of the "radius of influence" of the well and how far away the barrier, if any, would have to be by the end of the test. Single-well tests, which are more difficult to extract the well performance parameters from, are reduced by using a numerical technique based on a well in a porous medium. This numerical code allows a rough estimate of the minimum distance to barriers.

The following discussions of the radii of influence and the sensitivity of the well tests, coupled with the reduction of the single-well test data that are fitted using a numerical model based on porous flow, lead one to accept a model for flow through porous media as a reasonable representation of the system.

Radii of Influence

A well test examines the fluid in the rock for some distance away from the well. The distance into the rock that the test queries depends on the length of time the well is pumped or injected, and on the hydraulic properties of the rock, including transmissivity and storativity. In particular, boundaries, which are changes in the transmissivity, show up as changes in slope of the drawdown-versus-time curve in a pump test. Note that boundaries can be due to changes in hydraulic conductivity as a result of changes in either the depositional character of the rock being tested or as a result of alterations by fluids, perhaps with resulting induced fractures. The distance from a test well at which the initial head (drawdown) is essentially unchanged is called the radius of influence. Uncertainty in measurement makes the exact radius an imprecisely defined concept. Interpretation of the radius of influence is useful, however, because it gives some idea of the extent of the region being tested. It can tell whether or not there are hydraulic barriers (sources or changes in structure) and roughly how far from the test well they occur if present. It reveals gross inhomogeneities in the rock being tested. The results for the areal influence of pump tests performed in the Culebra as part of this study in 15 wells are summarized in Table A-1. The results indicate radii of influence of between ~37 and 1525 m (120 and 5000 ft) from the pumping source.

Two types of tests were performed: (a) two-well pump tests, and (b) the single-well pump tests. In the first case it is possible to calculate maximum and minimum distances to the "hydraulic barrier." For the second case, when there is a change in the slope of the drawdown curve, it is possible to calculate a distance

to the barrier; otherwise it is necessary to infer the distance from the numerical study of the well test. For the two-well pump test, an image of the pumping well is superimposed as a reflection across the hypothetical barrier. The configuration is as

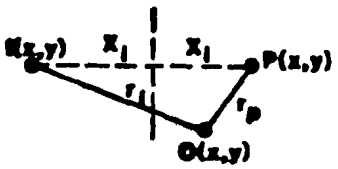

and

$$h = \frac{Q}{4\pi T}\left[W\left(\frac{r_p^2 S}{4Tt}\right) \pm W\left(\frac{r_i^2 S}{4Tt}\right)\right]$$

where h = head, W(u) is the exponential integral, in this form normally referred to as the well function, (Freeze and Cherry, 1979).

Table A-1. Summary of Results for the Areal Influence of Pump Tests Performed in the Culebra Unit

Test Well	Radii of Influence (ft)
H4A	929 - 829
H4B	1108 - 1008
H4C	216 - 119
5A	295 - 195
5B	334 - 234
5C	235 - 135
H-7B	Undetermined
H-8B	<500
H-9B	>500
P14	>5000
W25	<500
W26	>500
W27	>500
W28	<500
W30	>500

Q is the pumping rate, T is the transmissivity, r_p, r_i are the distances from the observation well O(x,y) to the pumping well P(x,y) and the image well L(x,y), respectively, S is the storativity, X_i is distance from the pumping well P to the barrier. In general, however, the orientation of the barrier is unknown, but extreme values can still be determined. That is, in the extreme one of the following two figures applies.

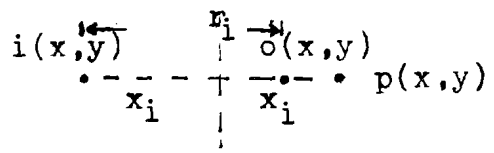

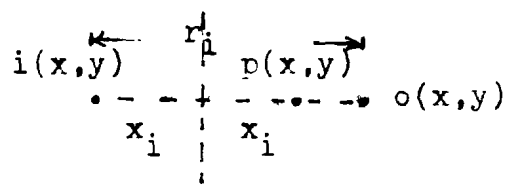

where

P is the pumping well, i is the image well, and O is the observation well as before.

For the three-test well complexes, H-4a, 4b, 4c, H-5a, 5b, 5c, H-6a, 6b, 6c, sites of pump tests were run in conjunction with the tracer and anisotropy studies at these sites (Ward et al, 1983). These pump tests exchanged pump and observation wells. In these tests, in general no unambiguous barriers were observed; thus what is calculated is rather the minimum distance a barrier would have to be from the pumping well in order for no barrier to be seen at the time the pump test ceased. The configuration for the H-4 complex is

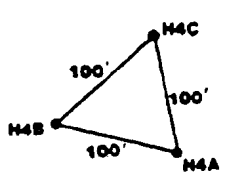

In Test 1, the pumped well was H-4b with H-4a, H-4c the observation wells. The hydraulic parameters are r_p = 100 ft, Q = 49.3 ft^3/d, t = 10^4 s, S(H-4a) = 3.13×10^{-6}, S(H-4c) = 5.67×10^{-6}, T(H-4a) = 1.18×10^{-3} ft^2/min, T(H-4c) = 1.042×10^{-3} ft^2/min, drawdown = 16 ft.

Then from the equation

$$h_o - h(r_p,t) = \frac{Q}{4\pi T}\left[W\left(\frac{r_p^2 S}{4Tt}\right) \pm W\left(\frac{r_i^2 S}{4Tt}\right)\right],$$

where the only unknown is V_i and from a table of well functions one computes $X_i = 216$ ft max or $X_i = 119$ ft min. For the observation well H-4a, one computes 283 ft $\geq X_i \geq$ 183 ft.

In Test 2, the pumped well was H-4c and the hydraulic parameters are T(H-4a) = 1.1 ft^2/d, T(H-4b) = 0.8 ft^2/d, S(H-4a) = 8.04×10^{-6}, S(H-4b) = 8.64×10^{-6}, Q = 61 ft^3/d, t = 3990 min, drawdown = 18.0 ft. Then one computes 708 ft $\geq X_i \geq$ 608 ft for observation well H-4a. When the observation well is H-4b, t = 2000 min, drawdown = 19 ft; then X_i is computed as 390 ft $\geq X_i \geq$ 290 ft.

In Test 3, the pumped well was H-4c and the hydraulic parameters are T(H-4a) = 1.3 ft^2/d, S(H-4a) = 5.62×10^{-6}, T(H-4b) = 1.2 ft^2/d, S(H-4b) = 6.48×10^{-6}, t = 4.5×10^3 min, drawdown = 22 ft, Q = 67.7 ft^3/d. The computed values for X_i are 929 ft > X_i > 829 ft for observation well H-4a and 1108 $\geq X_i \geq$ 1008 ft for observation well H-4b.

At complex H-5 the configuration is

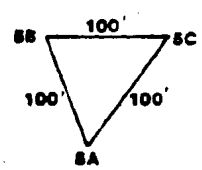

where similar tests were run. In Test 1, the pumping well was H-5b and the hydraulic parameters were T(H-5a) = 0.11 ft^2/d, S(H-5a) = 9.34×10^{-6}, T(H-5c) = 0.16 ft^2/d, S(H-5c) = 2.92×10^{-5}, Q = 34.6 ft^3/d, drawdown = 45 ft and t = 9000 min. In this case X_i is calculated as 235 ft $\geq X_i \geq$ 135 ft for observation well H-5c. In Test 2, the pumping well was H-5c and the hydraulic parameters were T(H-5a) = 0.15 ft^2/d, S(H-5a) = 2.5×10^{-5}, T(H-5b) = 0.12 ft^2/d, S(H-5b) = 2.6×10^{-5}, Q = 24.2 ft^3/d, drawdown = 35 ft, t ~1200 min. Then X_i is calculated as 295 ft $\geq X_i \geq$ 195 ft for observation well H-5a and 334 ft $\geq X_i \geq$ 234 ft for observation well H-5b.

For the well complex H-6, similar calculations were performed. Since this complex is still being studied comments will be deferred until the studies are complete.

The values computed here are not the minimum distance to an actual barrier but rather the minimum distance at which a barrier would have to be if the presence of a barrier had been noted at the end of the pump test. None of these tests on H-4 and H-5 actually showed the presence of a barrier. What the calculation does is provide an estimate of the distance around a test hole that is interrogated by the pump test and found not to have a detectable barrier. For this series of three-well tests, those distances varied from the order of 300 ft to 1300 ft.

Interpretation of Single-Well Data

Single-well pump tests are often carried out in the absence of any observation wells. In these cases the only data available are the pumping rate and the water level within the well as a function of time. From these data, transmissivities are deduced, usually by graphical means; that is, by matching the drawdown curve to standard type curves appropriate to certain aquifer conditions. Storativity is difficult to extract graphically, and sensitivity analyses of this deduced parameter are not generally possible. Data for these single-well pump tests are reduced here numerically. Such reduction allows investigation of the sensitivity of hydraulic conductivity and of the presence of possible barriers. The numerical model used is patterned after the analyses of Rushton and Redshaw (1979). A listing of our version of their analysis is given at the end of this section. Only wells in the Culebra are considered.

Single-Well Test Reduction

The mathematical model assumes that there is no vertical infiltration and that the following differential equation describes the drawdown. The differential equation for radial flow to a well is

$$\frac{\partial}{\partial r}\left(Kb\frac{\partial s}{\partial r}\right) + \frac{bK}{r}\frac{\partial s}{\partial r} = S\frac{\partial s}{\partial t} + q$$

where

s = drawdown (L)
r = radial coordinate (L)
b = thickness of the aquifer (L)
K = hydraulic conductivity (L/T)
S = storage coefficient
t = time (T)
q = recharge per unit area (L^3/L^2T)

A change of variable to $\zeta = \ln r$ is made so that the equation becomes

$$Kb \frac{\partial^2 s}{\partial \zeta^2} = Sr^2 \frac{\partial s}{\partial t} + qr^2 \quad .$$

The motivation for this change of variable is so that as finite-difference techniques are used to solve the equation, a regular mesh in ζ is a logarithmically increasing mesh in r. Then the region close to the pumping well, where rapid changes occur, is covered with more mesh points, and the region farther away with fewer. Likewise it is convenient to use logarithmically increasing time increments. The finite difference form of the equation at node n is

$$\frac{Kb}{\Delta\delta^2}(s_{n-1} - 2s_n + s_{n+1})_{t+\Delta t} = \frac{Sr_n^2}{\Delta t}(s_{n,t+\Delta t} - s_{n,t})$$

$$+ q_{t+1/2\Delta t}\, r_n^2$$

In keeping with Rushton and Redshaw's work (1979) the increment $\Delta\zeta$ was chosen as $\frac{1}{6}\ \ell_n$ (10) (0.3837641822) so that six mesh intervals occur for each tenfold increase in radius. From the radius of the well to 10 x is six intervals.

The equation is written in finite difference form as

$$\frac{T}{\Delta\delta^2}[D(N-1) - 2\,D(N) + D(N+1)] = \frac{Sr_n^2}{\Delta t}[D(N) - \text{OLD } D(N)] + Q * R(N) * R(N)$$

where

$s_{i,t}$ = OLD D(i)
$s_{i,t+\Delta t}$ = D(i)
$\Delta\zeta$ = mesh interval
$q_{t+1/2}$ = Q
Kb = T (transmissivity)

Derivation of the differential and difference equation considered only flow in the aquifer. However, since there is a well-bore that contains fluid, some special considerations must be given to the boundary and initial conditions implied by the presence of this fluid. Rushton and Redshaw (1979) handle the problem very cleverly by making the well-bore a part of the aquifer with altered transmissivity and storage coefficient.

Single-Well Tests

All tests performed in these wells have standard 5½-in.-dia casing. Their locations and geologic and hydraulic characteristics are described by Gonzalez (1983a). Initial values for the hydraulic conductivity were derived graphically by Gonzalez. Since determination of the storativity and of the sensitivity of the graphical solution for hydraulic conductivity are difficult for single-well tests, we followed the suggestion of Rushton and Redshaw (1979) and attempted to match drawdown curves or recovery curves by using a numerical method. In this method, attempts are made to match the experimentally determined drawdown curve by using the hydraulic conductivity determined graphically as a starting point. If the shapes of the two curves are geometrically similar, the storativity S is varied to obtain a match. If the shapes are not similiar, the hydraulic conductivity is varied to adjust the shape. In some cases the well radius was also adjusted to obtain a better short-time fit, which corrects for wellbore effects and development of the well. When a reasonable match is obtained, the value of the hydraulic conductivity is varied to establish a measure of the sensitivity of the interpretation to this parameter. Similarly, the storativity is varied for the same reason. Finally, the fixed outer boundary of the calculation that corresponds to a source is moved to obtain a rough value for the radius of influence of the test. In some cases where "residual" or "recovery" curves were available, the same techniques were applied to them.

The first set of the trials appears in the first figure in each group and shows the match to the data for different values of S and assumed a conductivity near that estimated graphically. The second figure in each group shows the match to the data for the value of S determined, but with varying K, hydraulic conductivity. The third figure in each group shows the change to the curve, if any, for fixed values of S and K but with different values of RMAX, the outer fixed radius in the problem, and offers a measure of the distance to a possible barrier. A barrier here is a constant-pressure fluid source. The wells that were examined in this way were WIPP 25 through WIPP 28, WIPP 30, P-14, H-7B, H-8B, and H-9B in the Culebra. Since not all of the wells behaved alike, they are discussed individually.

WIPP 25

Q (pumping rate) = 3.34 ft^3/min
K (hydraulic conductivity) = 7.36×10^{-3} ft/min (inferred graphically)
t (length of pump test) = 2000 min
Top of aquifer = 446 ft
Bottom of aquifer = 469 ft

Results of the numerical reduction of the data from WIPP25 appear in Figures A-1, A-2, and A-3. Figure A-1 shows the match for various values of storativity for K = 0.8×10^{-2}ft/min; it appears that a value of storativity of $\sim 0.1 \times 10^{-1}$ is a reasonable fit to this drawdown curve. Figure A-2 shows a comparison of values of K for a fixed storativity, and it is inferred that a good fit is obtained for K slightly larger than the value derived graphically. Figure A-3 shows the effect of a barrier at 5×10^2 ft and 5×10^3 ft; namely, there is no effect. A barrier would have to be closer than 500 ft for the numerical method to recognize it, given these data. The fit appears to be that of a classical drawdown test in a porous medium.

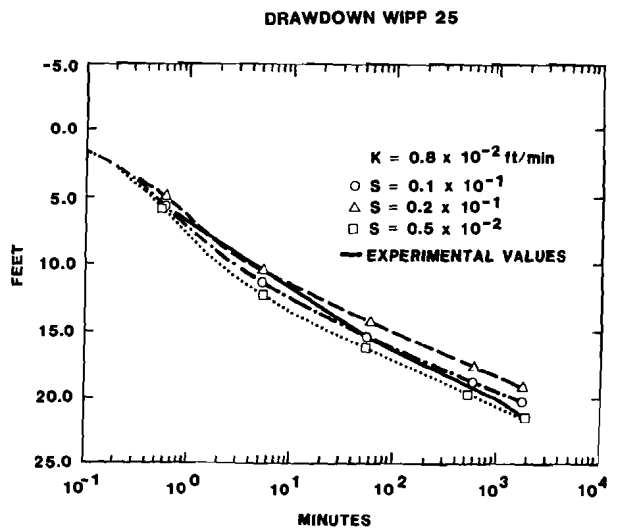

Figure A-2. Comparison of Hydraulic Conductivity for Fixed Storativity, WIPP 25

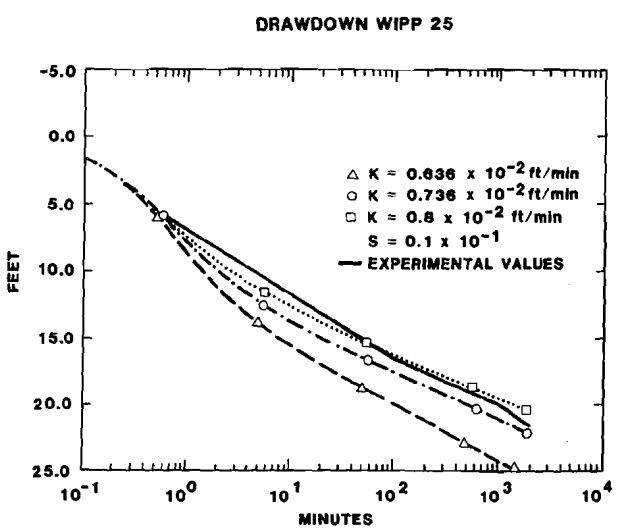

Figure A-1. Comparison of Storativity for Fixed Hydraulic Conductivity, WIPP 25

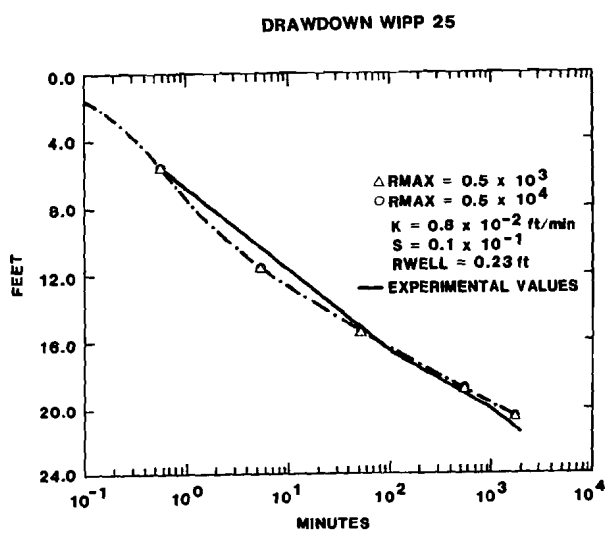

Figure A-3. Comparison of Influence of Outer Boundary of Problem, WIPP 25

WIPP 26

Q (pumping rate) = 4.545 ft^3/min
K (hydraulic conductivity) = 3.62×10^{-3} ft/min
t (length of pump test) = 2000 min
Top of aquifer = 186 ft
Bottom of aquifer = 209 ft

Results of the numerical reduction appear in Figures A-4, A-5, and A-6. Figure A-4 shows the match for various values of storativity for a hydraulic conductivity of 0.31×10^{-1} ft/min; the value of S of $\sim 0.48 \times 10^{-2}$ seems to be a reasonable fit. Figure A-5 displays values of K for a fixed S; here it is inferred that a good fit is obtained for a value of K $\sim$10 times larger than the value derived graphically. Figure A-6 displays the effect of a barrier at 5×10^2 ft and 5×10^3 ft. The barrier would have to be >500 ft away.

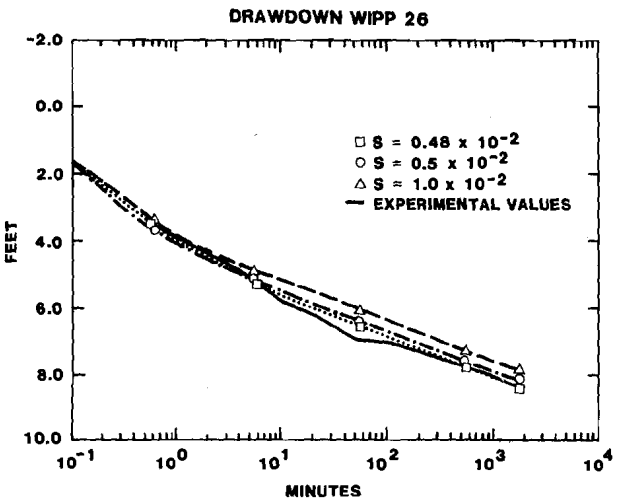

Figure A-4. Comparison of Storativity for Fixed Hydraulic Conductivity, WIPP 26

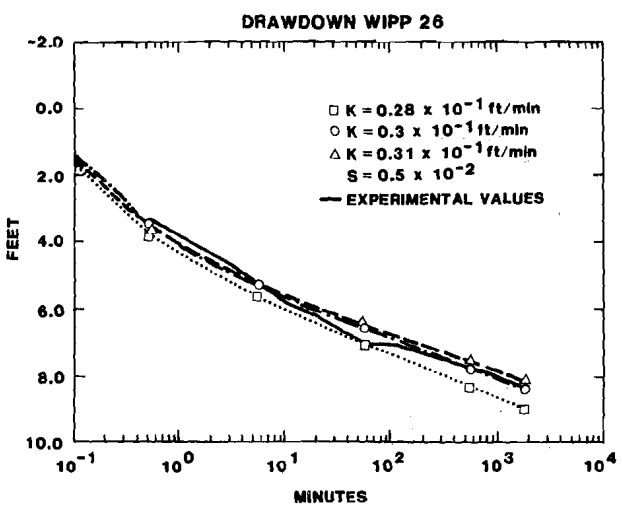

Figure A-5. Comparison of Hydraulic Conductivity for Fixed Storativity, WIPP 26

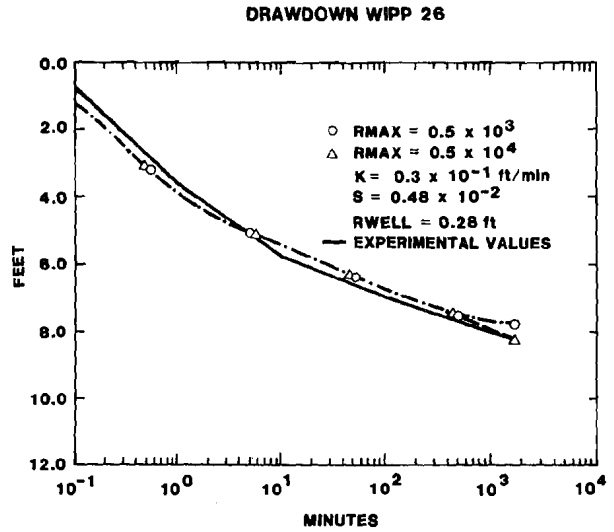

Figure A-6. Comparison of Influence of Outer Boundary of Problem, WIPP 26

WIPP 27

Q (pumping rate) = 3.34 ft^3/min
K (hydraulic conductivity) = 2.28×10^{-3} ft/min
t (length of pump test) = 2000 min
Top of aquifer = 292 ft
Bottom of aquifer = 318 ft

Results of the numerical reduction appear in Figures A-7, A-8, and A-9. Figure A-7 shows the match for various values of storativity for a hydraulic conductivity of 0.65×10^{-2} ft/min. None of the storativity values match the fluctuations around 200 min; however, the best overall fit appears to be $\sim S = 0.1 \times 10^{-5}$ for a well radius of 0.18 ft. The cause for the fluctuations is at present unknown and requires more investigation. The well radius was adjusted to allow better match at short times and in recognition of the fact that not all wells have an effective radius equal to the nominal cased value. Figure A-8 shows the values of K for a fixed S; it appears that a value of $K = 0.65 \times 10^{-2}$ ft/min is a reasonable fit. Figure A-9 shows the effect of a barrier at 5×10^2 ft and 5×10^3 ft. The barrier would have to be >500 ft away.

WIPP 28

Q (pumping rate) = 2.33 ft^3/min
K (hydraulic conductivity) = 5.17×10^{-4} ft/min
t (length of pump test) = 350 min
Top of aquifer = 420 ft
Bottom of aquifer = 446 ft

Results of the numerical reduction appear in Figures A-10, A-11, and A-12. Figure A-10 shows the

match for various values of storativity for a hydraulic conductivity of 0.55×10^{-3} ft/min. The match is relatively poor for short times and suggests that $S = 0.5 \times 10^{-1}$ is appropriate for long times. However, variation of effective well radius for the same hydraulic conductivity makes it clear that $S = 0.1$, and a well radius of 0.2 give a closer approximation (see Figure A-11) than does the nominal well radius, 0.23 ft. The values on Figure A-12 compare various values of K for a fixed S. It appears that $K = 0.55 \times 10^{-3}$ ft/min supplies a reasonable fit. Figure A-13 shows the results of moving the problem boundary to 0.5×10^{3} ft; there is no difference from the boundary at 0.5×10^{4} ft, thus any barrier would have to be at a lesser minimum distance.

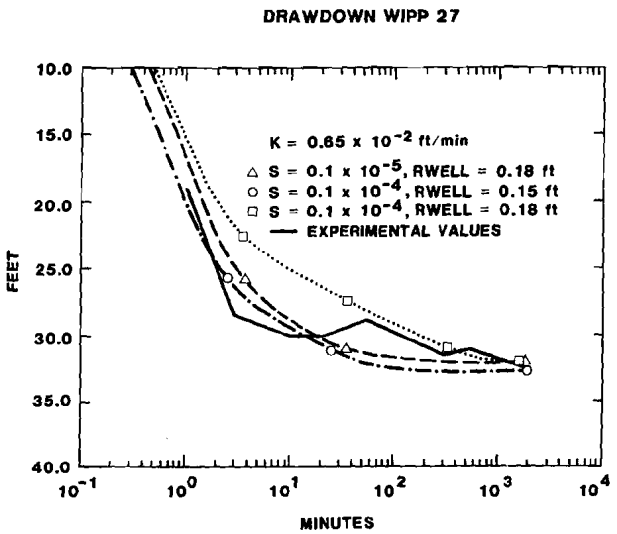

Figure A-7. Comparison of Storativity for Fixed Hydraulic Conductivity, WIPP 27

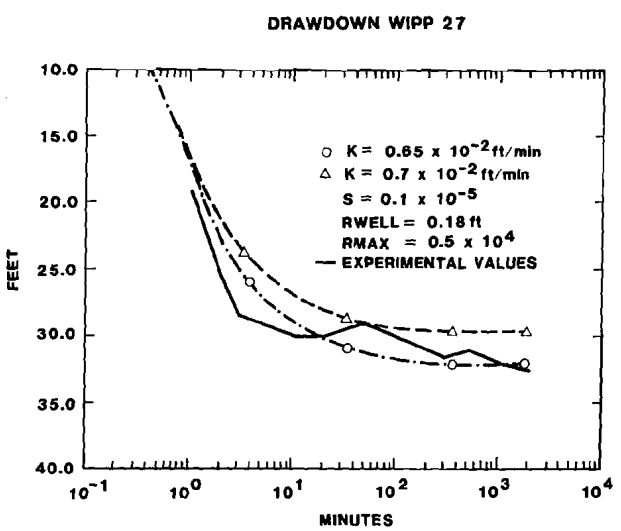

Figure A-8. Comparison of Hydraulic Conductivity for Fixed Storativity, WIPP 27

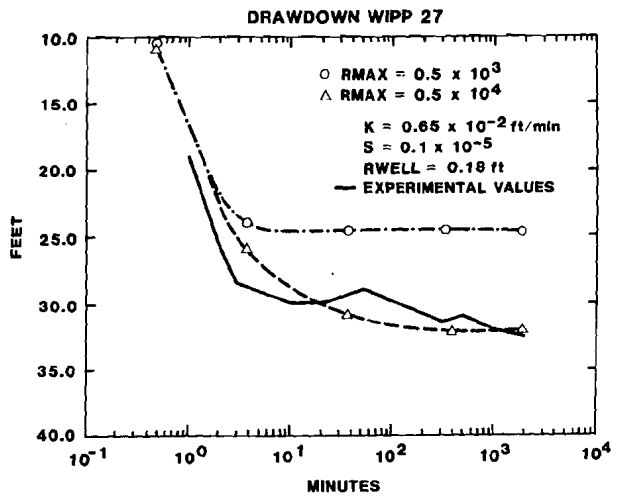

Figure A-9. Comparison of Influence of Outer Boundary of Problem, WIPP 27

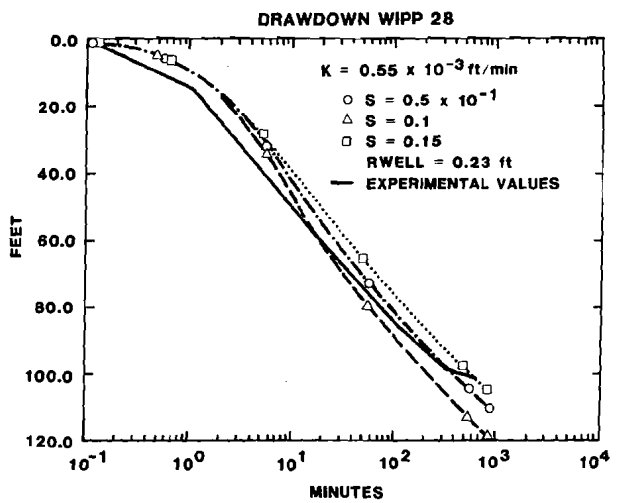

Figure A-10. Comparison of Storativity for Fixed Hydraulic Conductivity, WIPP 28

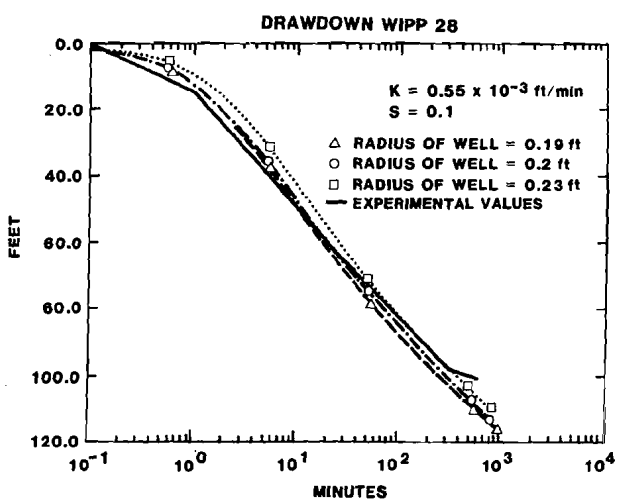

Figure A-11. Comparison of Effect of Variation of Well Radius, WIPP 28

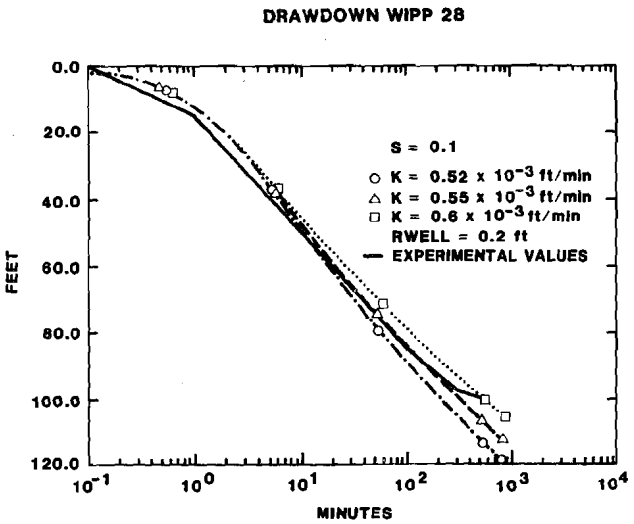

Figure A-12. Comparison of Hydraulic Conductivity for Fixed Storativity, WIPP 28

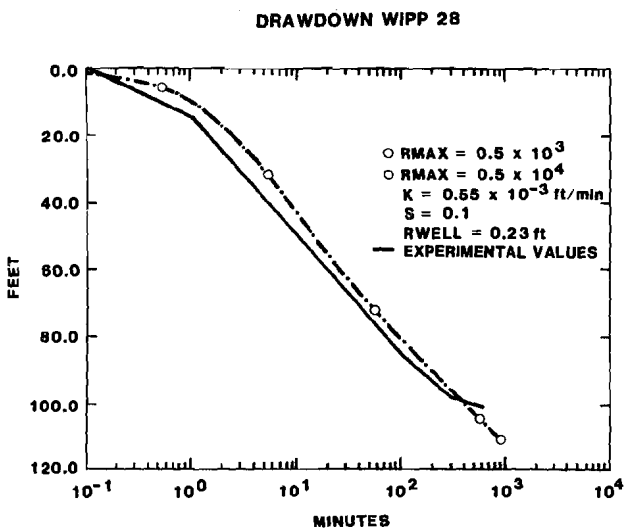

Figure A-13. Comparison of Influence of Outer Boundary of Problem, WIPP 28

WIPP 30

Q (pumping rate) = 4.025×10^{-2}
K (hydraulic conductivity) = 0.631×10^{-6} ft/min
t (length of pump test) = 500 min
Top of aquifer = 631 ft
Bottom of aquifer = 653 ft

The drawdown at this test well was so rapid that it was possible to match the results numerically with virtually any storativity within 2 orders of magnitude of 0.5×10^{-4}. This drawdown curve and a numerical match are shown in Figure A-14. For this reason it was necessary to turn to the recovery (or residual curve). The code used for numerical reduction accepts recovery (see input instructions). Figure A-15 shows a comparison for fixed K (0.6×10^{-3}) and varying S. The match is relatively insensitive to S. The short time departure from the experimental curve occurs because of a relatively poor match for the initial drawdown data, which were left uncorrected to better illustrate the eventual match. More careful selection of the initial drawdown data provided a much better fit for short times. Figure A-16 illustrates the effect of varying K; note that the inferred value of K differs from the original supposition. The comparison for a restricted boundary at 0.5×10^3 ft with the maximum radius of 0.5×10^4 ft produces a change, but so small that it cannot be represented on the graph. Therefore the figure is omitted, and the boundary must be at least 500 ft away.

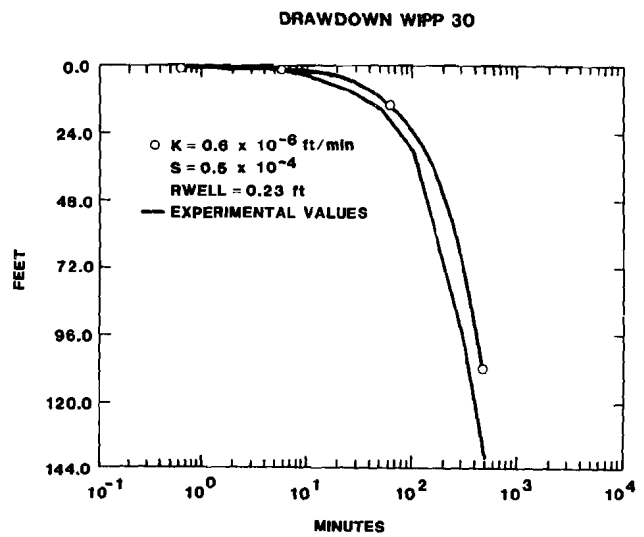

Figure A-14. Example of the Match to Drawdown for Arbitrary Hydraulic Conductivity, WIPP 30

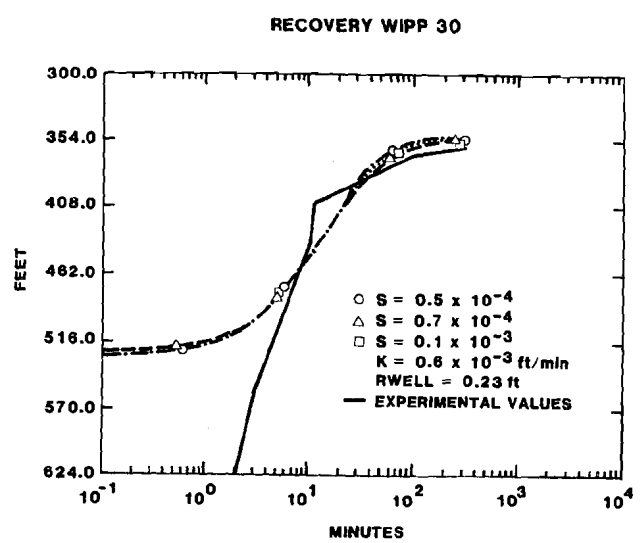

Figure A-15. Comparison of Storativity for Fixed Hydraulic Conductivity, WIPP 30

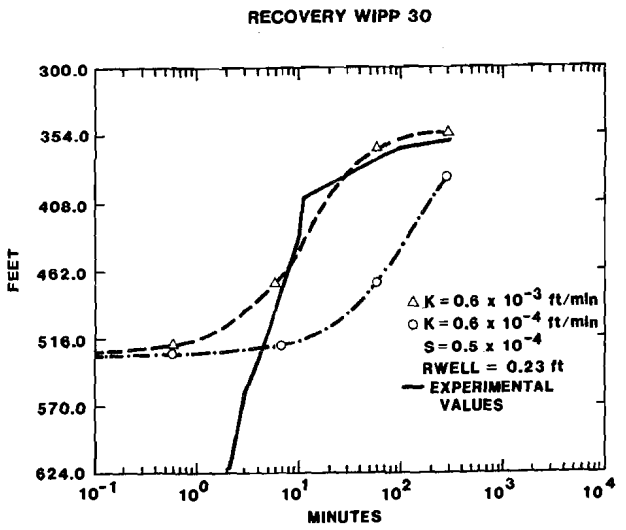

Figure A-16. Comparison of Hydraulic Conductivity for Fixed Storativity, WIPP 30

P-14

Q (pumping rate) = 1.376 ft^3/min
K (hydraulic conductivity) = 1.91 $\times$ 10^{-2} ft/min
t (duration of test) = 800 min
Top of aquifer = 573 ft
Bottom of aquifer = 595 ft

Results of the numerical reduction are illustrated in Figures A-17, A-18, and A-19. Figure A-17 shows the match at a fixed hydraulic conductivity for varying storativity. The range of values is fairly restricted, and the inferred value is 0.2 $\times$ 10^{-4}. The effective well radius was reduced to 0.15 ft to improve the fit with respect to very early data. Figure A-18 illustrates the match at a fixed storativity and varying hydraulic conductivities; the value with the best fit appears to be K = 0.15 $\times$ 10^{-1} ft/min, a small departure from the graphical value of 1.9 $\times$ 10^{-2}. Figure A-19 shows the effect of altering the boundary of the calculation; a very slight change occurs at long times. This suggests that any barrier must be at least 5. $\times$ 10^3 ft away.

H-7b

Q (pumping rate) = 12.03 ft^3/min
K (hydraulic conductivity) = 0.12 ft/min
t (duration of test) = 100 min
Top of aquifer = 237 ft
Bottom of aquifer = 283 ft

Results of numerical reduction have so far been unsatisfactory for this well. The hydraulic conductivity appears to be ~0.35 $\times$ 10^{-1} and the storativity ~0.5 $\times$ 10^{-6}. The primary means of matching to the drawdown curve has been by variation of the well diameter. Several of those matches are shown in Figure A-20. Better matching may require introduction of a barrier nearby or other factors such as delayed yield or leakage into the numerical model. At the moment the drawdown behavior has not been resolved numerically, but more field tests are planned.

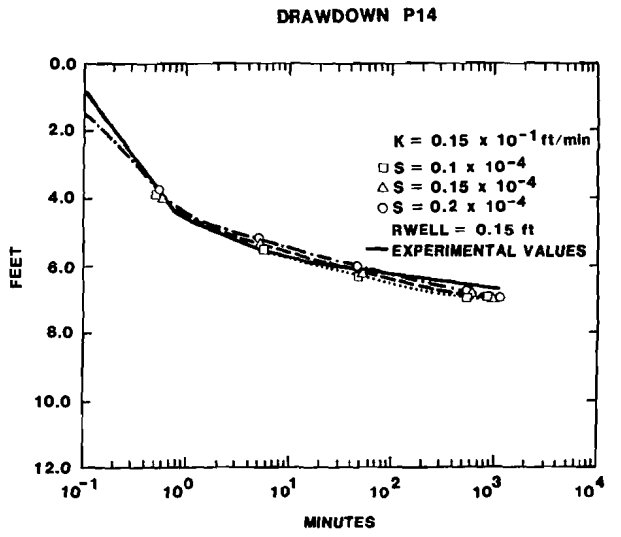

Figure A-17. Comparison of Storativity for Fixed Hydraulic Conductivity, P14

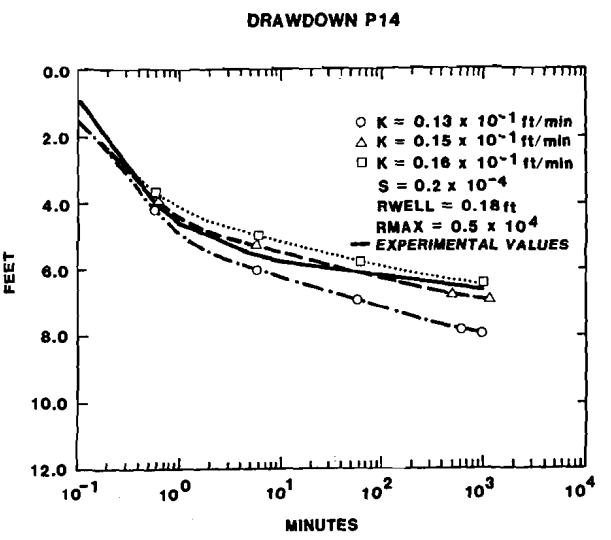

Figure A-18. Comparison of Hydraulic Conductivity for Fixed Storativity, P14

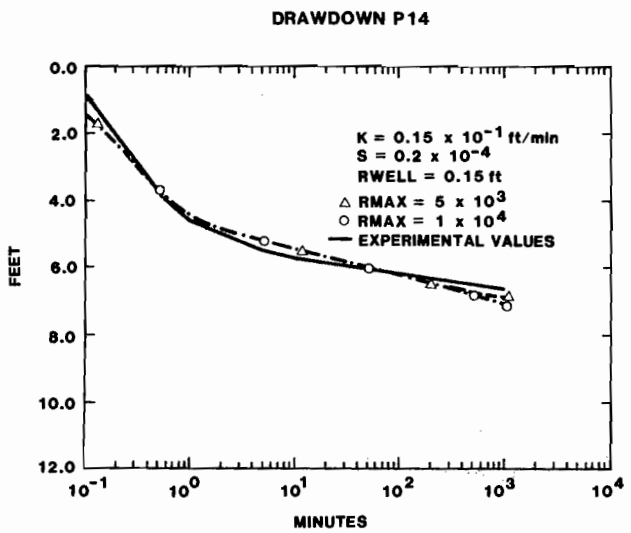

Figure A-19. Comparison of Influence of Outer Boundary of Problem, P14

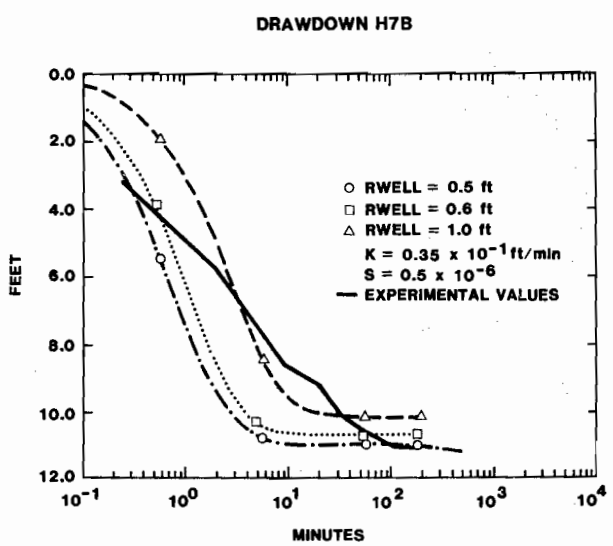

Figure A-20. Comparison of Various Well Sizes for Fixed Hydraulic Conductivity and Storativity, H7b

H-8b

Q (pumping rate) = 2.14 ft^3/min
K (hydraulic conductivity) = 0.173 ft/min
t (duration of test) = 600 min
Top of aquifer = 586 ft
Bottom of aquifer = 613 ft

Results of numerical reduction are illustrated in Figures A-21, A-22, and A-23. Figure A-21 shows the results for fixed K and variable S, for a well radius of 0.18 ft. The match is not totally satisfactory, particularly at small times, but nonetheless an approximate value of $S = 0.1 \times 10^{-1}$ is inferred. Figure A-22 shows the match for fixed S and variable K. The inferred value of K is 0.25×10^{-2} ft/min. For the effect of the boundary, Figure A-23, which was calculated with different values of K and S than those decided here ($K = 0.29 \times 10^{-2}$, $S = 0.5 \times 10^{-2}$), is the same for RMAX $= 0.5 \times 10^3$ ft and 0.5×10^4 ft.

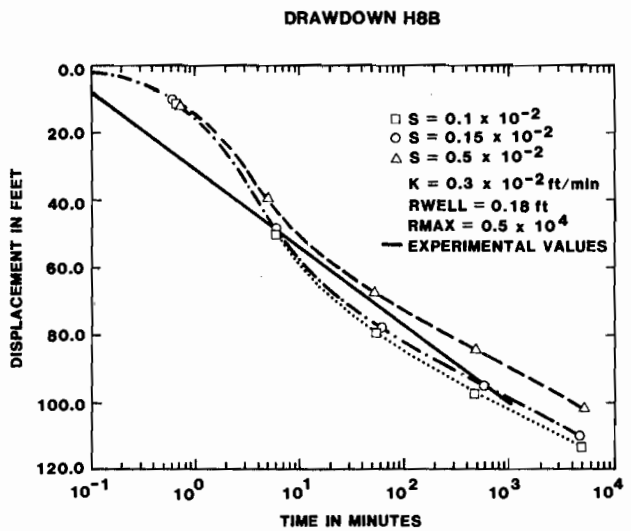

Figure A-21. Comparison of Storativity for Fixed Hydraulic Conductivity, H8b

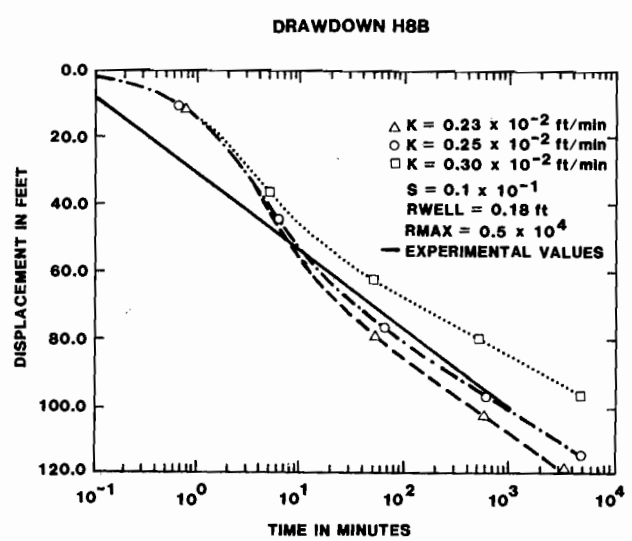

Figure A-22. Comparison of Hydraulic Conductivity for Fixed Storativity, H8b

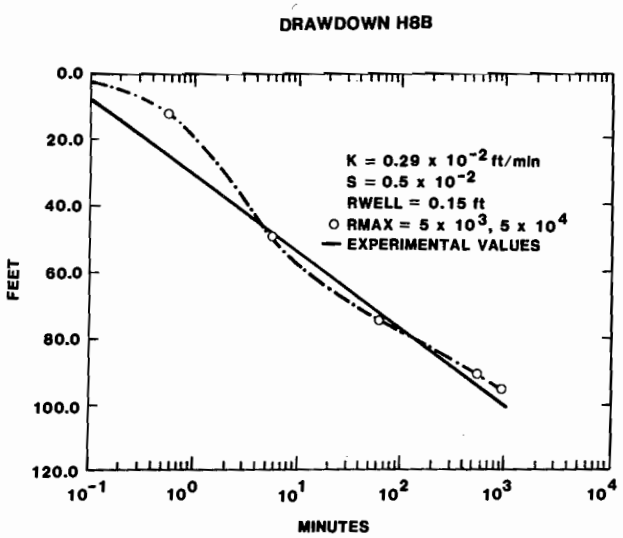

Figure A-23. Comparison of Influence of Outer Boundary of Problem, H8b

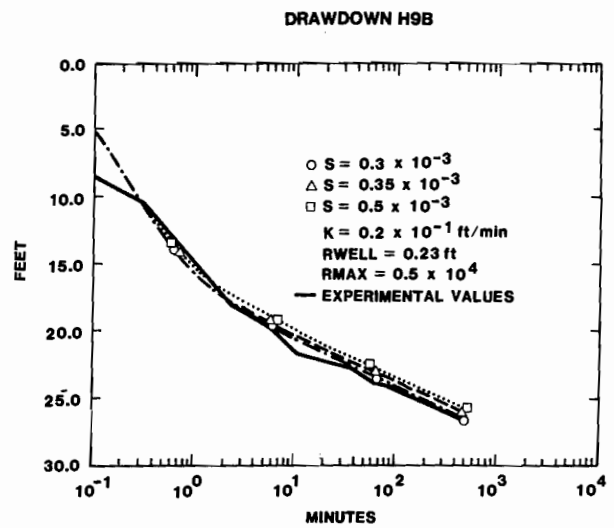

Figure A-24. Comparison of Storativity for Fixed Hydraulic Conductivity, H9b

H-9b

Q (pumping rate) = 11.83 ft^3/min
K (hydraulic conductivity) = 4.68×10^{-3} ft/min
t (duration of test) = 200 min
Top of aquifer = 523 ft
Bottom of aquifer = 554 ft

Results of numerical reduction are illustrated in Figures A-24, A-25, and A-26. Figure A-24 shows the results for fixed K and varying S; the inferred value of S is 0.35×10^{-3}. Figure A-25 shows the results for fixed S and varying K, with the inferred value for K being 0.2×10^{-1} ft/min. Figure A-26 shows the comparison of drawdown for different values of RMAX and the upturn of values for RMAX = 0.5×10^3 ft; and absence of movement for RMAX = 0.5×10^4 ft suggests no barrier in that range.

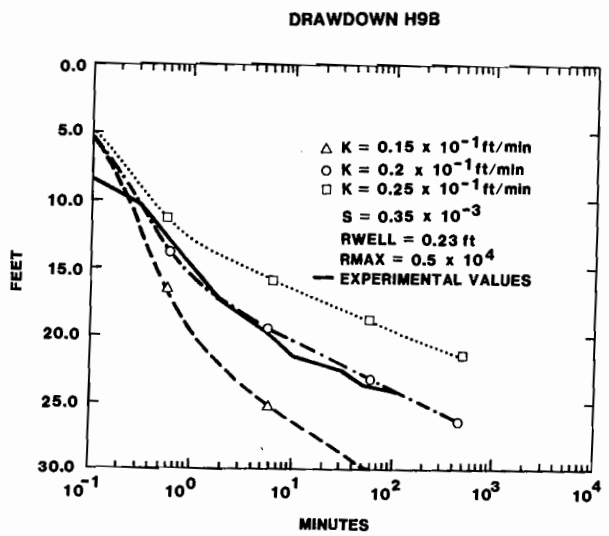

Figure A-25. Comparison of Hydraulic Conductivity for Fixed Storativity, H9b

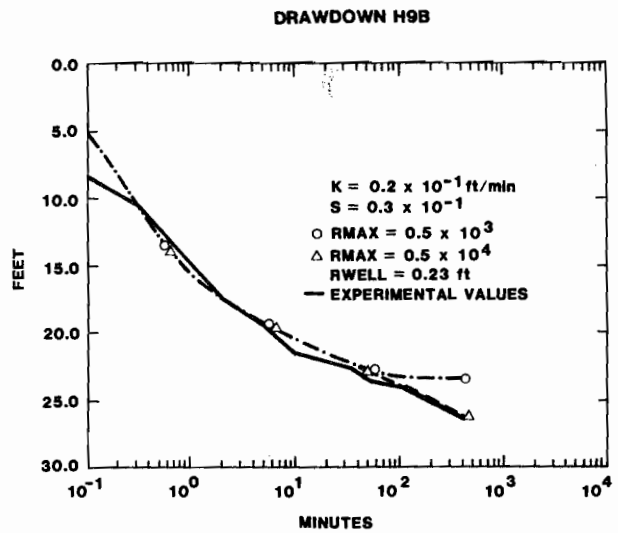

Figure A-26. Comparison of Influence of Outer Boundary of Problem, H9b

Conclusion for Analyses of Supporting Data

The choice of the mathematical representation of flow by a model dependent on flow through porous media, through fractures, or through some combination of the two, depends on the analysis of field data. A porous medium was initially chosen here, on the basis of examination of core from the Rustler Dolomites and on field interpretation of aquifer pump tests. For the wells discussed here, in general their drawdown behaviors were consistent with representation of the Culebra as a porous medium. Inconsistency as in H-7b is being studied, but since the Culebra appears to be well-fractured and the fractures filled with a second porous medium, some occasional local inconsistency should be expected. The general characteristics of core from the Magenta and Culebra are discussed by Gonzalez (1983a).

Input for PUMP Code

Card 1		
M,K	2I5	M = −1 for drawdown
		= 0 for recovery
		K = Number of terms for data for recovery
Card 2		
N	I5	Number of value pairs for experimental drawdown or Recovery curve
Card 3		
STDTIME (I), STDANS(I)	*	Time of drawdown datum, drawdown or recovery values (N)
Card 4		
COND,SCON,	3F10.5	Hydraulic conductivity, storativity
Card 5		
RWELL	2F10.5	Well radius
RMAX		Maximum radius of problem
Card 6		
TOP,		Top of aquifer measured from surface
BASE,	4F10.5	Base of aquifer measured from surface
WLEVEL		Water level of aquifer measured from surface
RCH		Recharge
Card Set 7		
D(I)	8F10.3	Initial drawdown for recovery, K in number
Card Set 8		
OLD D(I)	8F10.3	Previous initial drawdown for recovery, K in number
Card 9		
JFIX	I1	= 1 for a fixed outer boundary (RMAX)
		= 0 for a free outer boundary
Card 10		
NOB	6I3	Node numbers of six observation wells
Card 11		
QPUMP	2F10.3	QPUMP = pumping rate (=0. for recovery)
TSTOP		TSTOP = time at which pumping is stopped

```
INPUT FOR WIPP28   DRAWDOWN
    7
 0.1 0.0  1.0 15.0  10.0 51.0  100.0 85.0  200.0 93.0  300.0 98.0  600.0 101.0
  .550E-03  .100E-00   1.0E-05
   .46E-00   .50E+04
 .4200E+03  .446E+03  .000E+00   1.0E-21
1
  1  2 05 10 25 30
  2.330000  .100E+04
    -1.0       0.0
END OF FILE
>?
```

```
INPUT FOR USWH1 TEST1    RECOVERY
    0   16
   12
1.0 501.10 2.0 501.0 4.0 500.87 9.0 500.75 20.0 500.63 40.0 500.5 80.0 500.37
200. 500.2 400. 500.13 600. 500.09 1000. 500.02  2500. 500.
  1.00E-03 0.500E-00
 0.23E-00  0.500E+03
  5.72E+02  6.88E+02  5.00E+02  1.00E-20
 5.0144E+2 5.0144E+2 5.0133E+2 5.0122E+2 5.0111E+2 5.0101E+2 5.0089E+2 5.0079E+2
 5.0068E+2 5.0058E+2 5.0047E+2 5.0037E+2 5.0027E+2 5.0017E+2 5.0009E+2 5.0000E+2
 5.0144E+2 5.0144E+2 5.0133E+2 5.0122E+2 5.0111E+2 5.0101E+2 5.0089E+2 5.0079E+2
 5.0068E+2 5.0058E+2 5.0047E+2 5.0037E+2 5.0027E+2 5.0017E+2 5.0009E+2 5.0000E+2
1
  1  2  5 10 25 30
 0.000E+00  3.00E+03
   -1.0        0.0
END OF FILE
>?
```

LISTING OF THE CODE NEWPUMP TO REDUCE THE PUMPTEST DATA FOR THE SINGLE-WELL TESTS

```
00100 PROGRAM NEWPUMP (INPUT=101B,OUTPUT=101B,TAPE77,
00110+                TAPE66=INPUT, TAPE0,TAPE1,TAPE2)
00120C-----------------------------------------------------------------
00130C---INPUT FILE = TAPE1
00140C---OUTPUT FILE = TAPE2
00150C
00160C   TO EXECUTE THIS PROGRAM FROM A 4014 TERMINAL AT SNL:
00170C
00180C      1) MAKE PROGRAM 'NEWPUMP' THE PRIMARY FILE, AND
00190C         MAKE THE INPUT FILE 'TAPE1' A LOCAL FILE.
00200C      2) IN THE 'FTNTS' SUBSYSTEM TYPE;
00210C            RUN,B=LGO
00220C      3) CHANGE TO THE 'BATCH' SUBSYSTEM AND TYPE;
00230C            A) RA
00240C            B) DISS,TK4,F=F4
00250C
00260C      AND IN A LITTLE WHILE A GRAPH WILL BEGIN TO APPEAR ON
00270C      THE SCREEN......
00280C                                                          1-7-83
00290C-----------------------------------------------------------------
00300C
00310C  NUMERICAL PUMPING TEST, NO VERTICAL FLOW, WATER IN WELL
00320C
00330 DIMENSION R(100),RR(100),D(100),OLDD(100),T(100),H(100),RECH(100),
00340+ A(100),B(100),C(100),E(100),U(100),V(100),NOB(6),ARRAY(6),
00350+  STDTIME(20), STDANS(20), CALTIME(200), CALANS(200)
00360C
00361 READ (1,997) M,K
00362 997 FORMAT (2I5)
00363C M=-1 FOR PUMP TEST, M=0 FOR RECOVERY.
00370 READ (1,999) N
00380 999 FORMAT (I5)
00390 READ (1,*) (STDTIME(I), STDANS(I), I=1,N)
00400C
00410 CALL VSTART (0.,0)
00411 IF (M .LT. 0) GO TO 2420
00412 CALL TITLE (17H RECOVERY WIPP 30,-17,10H MINUTES  ,11,
00413+              21H          FEET         ,21,8.0,6.0)
00414 GO TO 2440
00420 2420 CALL TITLE(17HDRAW DOWN WIPP 26,-17,15HTIME IN MINUTES,15
00430+            ,21HDISSPLACEMENT IN FEET,21,8.0,6.0)
00440 2440 CALL XLOG (0.1,1.6,12.0,-2.0)
00450 CALL CURVE (STDTIME,STDANS,N,0)
00460 CALL SETDEV (0,0)
00470 ICOUNT=0
00480C
00490C  INPUT AQUIFER PARAMETERS
00500C
00510 READ (1,510) COND,SCON
00520 510 FORMAT (4F10.5)
00530 WRITE (2,515) COND,SCON
00540 515 FORMAT (1X,14HCONDUCTIVITY =  ,E12.4,19H  CONFINED STORAGE=  ,
00550+ E12.4)
00560C
00570C INPUT OF RADII AND SETTING UP THE MESH
```

```
00580C
00590  READ (1,500) RWELL,RMAX
00600 500 FORMAT (2F10.3)
00610 WRITE (2,505) RWELL,RMAX
00620 505 FORMAT (1X,14HWELL RADIUS =   ,E12.4,13H  MAX RADIUS=  ,E12.4)
00630C
00640C SET UP RADIAL MESH
00650C
00660 DO 10 N=1,100
00670     AN=0.16666666667*FLOAT(N-2)
00680     R(N)=RWELL*10.0**AN
00690     IF(   R(N).LT.RMAX) GO TO 10
00700     R(N)=RMAX
00710     RR(N)=RMAX*RMAX
00720     NMAX=N
00730     NMONE=N-1
00740     GO TO 20
00750 10 RR(N)=R(N)*R(N)
00760 20 DELA=0.383765
00770 DELA2=DELA*DELA
00780C
00790C LEVELS MEASURED BELOW DATUM
00800C
00810 READ (1,520) TOP,BASE,WLEVEL,RCH
00820 520 FORMAT(4F10.5)
00830 WRITE (2,525) TOP,BASE,WLEVEL,RCH
00840 525 FORMAT (1X,16HTOP OF AQUIFER  ,E12.4,17H  BASE OF AQUIFER   ,
00850+ E12.4,22H INITIAL WATER LEVEL=  ,E12.4,11HRECHARGE=  ,E12.4)
00860C
00870C SET INITIAL CONDITIONS
00880C
00890 DO 30 N=1,NMAX
00900     RECH(N)=RCH
00910     D(N)=WLEVEL
00920 30 OLDD(N)=WLEVEL
00921 IF (M .LT. 0) GO TO 2929
00922 READ (1,998) (D(I),I=1,K)
00923 READ (1,998) (OLDD(I),I=1,K)
00924 998 FORMAT (8F10.3)
00929 2929 CONTINUE
00930C
00940C CONDITIONS ON OUTER BOUNDARY
00950C
00960C IF JFIX=1 LEVEL AT OUTER BOUNDARY REMAINS AT WLEVEL
00970C
00980 READ (1,530) JFIX
00990 530 FORMAT (I1)
01000 IF (JFIX.EQ.1) WRITE (2,532)
01010 IF (JFIX.NE.1) WRITE (2,534)
01020 532 FORMAT (22H  ** FIXED BOUNDARY**   )
01030 534 FORMAT (22H  ** FREE BOUNDARY **  )
01040C
01050C GIVE NODE NUMBER OF SIX OBS WELLS
01060C
```

```
01070 READ (1,540) (NOB(J),J=1,6)
01080 540 FORMAT (6I3)
01090C
01100C INPUT ABSTRACTION RATE
01110C
01120 TSTART=0.0
01130 READ (1,550) QPUMP,TSTOP
01140 550 FORMAT (2F10.3)
01150 WRITE (2,555) QPUMP,TSTOP
01160 555 FORMAT(1X,15HPUMPING RATE=   ,E12.4,14H TILL TIME OF   ,E12.4,
01170+ 5H MINS   )
01180C
01190C CONVERTING ABSTARCTION RATE TO QABST
01200C
01210 PI=4.0*ATAN(1.0)
01220 QABST=0.5*QPUMP/(PI*DELA)
01230 IND=0
01240C
01250C INTIAL TIME AND DELT
01260C
01270 TIME=0.0
01280 DELI=0.025*RR(1)*SCON/(COND*(BASE-TOP))
01290 DELT=DELI
01300 DO 35 I=1,6
01310    I1=NOB(I)
01320 35 ARRAY(I)=R(I1)
01330 WRITE (2,545) R(1),(ARRAY(J),J=1,6),R(NMAX)
01340 545 FORMAT(1X,24HTIME  (MINS)                    ,8F12.4)
01350C
01360C CALCULATION FOR A SPECIFIC TIME, IND=0 FOR LAST STEP
01370C
01380 40 TIME=TIME + DELT
01390 IF(TIME.LT.TSTOP) GO TO 50
01400 DELT=TSTOP-TIME+DELT
01410 TIME=TSTOP
01420 IND=100
01430C
01440 50 CONTINUE
01450C
01460C CALCULATION REPEATED FOUR TIMES FOR CONVERGENCE
01470C
01480 DO 60 NUM=1,4
01490 DO 70 N=1,NMONE
01500C
01510C TAKE AVERAGE SATURATED DEPTH BETWEEN N AND N+1
01520C
01530 SD=BASE-0.5*(D(N)+D(N+1))
01560 SD=BASE - TOP
01570 STOR=SCON
01580 H(N) = DELA2/(SD*COND)
01590 70 T(N)=DELT/(STOR*RR(N))
01600C
01610C TO REPRESENT WATER IN WELL
01620C
```

```
01630 H(1)=0.0001*H(1)
01640 T(1)=2.0*DELT*DELA/RR(2)
01650 T(2)=2.0*T(2)
01660 H(NMAX-1)=(ALOG(R(NMAX))-ALOG(R(NMAX-1)))*(ALOG(R(NMAX))-ALOG
01670+ (R(NMAX-1)))/(SD*COND)
01680 H(NMAX)=1.0E+10
01690 T(NMONE)=2.0*DELT*DELA/((R(NMAX)-R(NMONE-1))*STOR*R(NMONE))
01700 T(NMAX )=1.0*DELT*DELA/((R(NMAX)-R(NMONE))*STOR*R(NMAX))
01710 IF (JFIX.EQ.1) T(NMAX)=1.0E-10*T(NMAX)
01720C
01730C GAUSSIAN ELIMINATION
01740C
01750C CALCULATION OF COEFFICIENTS
01760C EQUN IS -A(N)*D(N-1) + B(N)*D(N) - C(N)*D(N+1) = E(N)
01770C
01780 B(1)=1.0/H(1) +1.0/T(1)
01790 C(1)=1.0/H(1)
01800 E(1)=OLDD(1)/T(1) + QABST
01810 DO 90 N=2,NMONE
01820    A(N)=1.0/H(N-1)
01830    B(N)=1.0/H(N-1) + 1.0/H(N) + 1.0/T(N)
01840    C(N)=1.0/H(N)
01850 90 E(N)=OLDD(N)/T(N) - RR(N)*RECH(N)
01860 A(NMAX)=1.0/H(NMONE)
01870 B(NMAX)=1.0/H(NMONE) + 0.5/T(NMAX)
01880 E(NMAX)=0.5*OLDD(NMAX)/T(NMAX) - 0.5*RR(NMAX)*RECH(NMAX)
01890C
01900C ELIMINATION
01910C
01920 U(1)=B(1)
01930 V(1)=E(1)
01940 DO 100 N=2,NMAX
01950    U(N)=B(N) - (A(N)*C(N-1))/U(N-1)
01960 100 V(N)=E(N) + (A(N)*V(N-1))/U(N-1)
01970 D(NMAX)=V(NMAX)/U(NMAX)
01980 DO 110 NN=1,NMONE
01990     N=NMONE-NN+1
02000 110 D(N)=(V(N) + C(N)*D(N+1))/U(N)
02010C
02020C TEST FOR EXCESSIVE DRAWDOWNS
02030C
02040 DRAWMX=0.9*BASE + 0.1*TOP
02050 IF (D(1).LT.DRAWMX) GO TO 60
02060 WRITE (2,580)
02070 580 FORMAT (1X,20H EXCESSIVE DRAWDOWN  )
02080 WRITE (2,565)
02090 DO 105 N=1,NMAX
02100 105 WRITE (2,570) N,R(N),H(N),T(N),D(N)
02110 STOP
02120C
02130 60 CONTINUE
02140C
02150C OUTPUT AND CHANGE PARAMETERS
02160C
```

```
02170 TIMIN=TIME - TSTART
02180 DO 120 I=1,6
02190      I1=NOD(I)
02200 120 ARRAY(I)=D(I1)
02210 ICOUNT = ICOUNT + 1
02220 IF(ICOUNT.GT.200) GO TO 125
02230 CALTIME(ICOUNT) = TIME
02240 CALANS (ICOUNT) = D(1)
02250 125 CONTINUE
02260C
02270C
02280 WRITE (2,560) TIME,TIMIN,D(1),(ARRAY(J),J=1,6),D(NMAX)
02290 560 FORMAT (1X,10E12.4)
02300 DO 130 N=1,NMAX
02310 130 OLDD(N)=D(N)
02320 DELT=TIMIN*0.25892
02330 IF (IND.EQ.0) GO TO 40
02340C
02350C END OF CALCULATIONS FOR A SPECIFIC TIME
02360C
02370 WRITE (2,565)
02380 565 FORMAT (1X,8HNODE NO.,4X,6HRADIUS,6X,8HDRAWDOWN)
02400 DO 140 N=1,NMAX
02410 140 WRITE (2,570) N,R(N),RR(N),H(N),T(N),OLDD(N)
02420 570 FORMAT (1X,I4,5E20.6)
02550 IF (ICOUNT.GT.200)  ICOUNT = 201
02560 ICOUNT = ICOUNT - 1
02570C
02571 IF ( M .EQ. 0) GO TO 2611
02590 DO 150 I=1,ICOUNT
02600 150 CALANS(I) = CALANS(I) - WLEVEL
02610C
02611 2611 CONTINUE
02620 CALL CURVE (CALTIME,CALANS,ICOUNT,10)
02630 CALL STRTPT (0.0,0.0)
02640 CALL ENDPL
02650 CALL DONEPL
02660C
02670 STOP
02680 END
END OF FILE
```

APPENDIX B

Comparison With the Hydraulic Model Used in the FEIS

During preparation of the FEIS, INTERA constructed a model for the hydraulics for the region around the WIPP site. Their model covered a region of 36 × 36 mi, with the WIPP site located about 8 mi east and 2 mi north of the center. Here the term model applies to the hydraulic description of the site including the computer code. INTERA, based on the best available data at that time, assigned hydraulic conductivities as shown in Figure B-1 and assumed hydraulic (head) potentials as shown in Figure B-2 (US DOE, 1980). INTERA's calculations were duplicated by PNL (Cole and Bond, 1980) and were shown to be essentially independent of the computer code. At the time of INTERA's calculations the hydraulic data were not available to distinguish between the two units of the Rustler, the Culebra and the Magenta. For this reason, the combined data for the two units were modeled as a single aquifer, the Rustler. Further, since the heads suggested that there was a gradient toward Malaga Bend on the Pecos River, it was decided to assume that the influx of saline fluids to the Pecos at Malaga Bend would also be the nearest outfall for contaminates for the WIPP site. This assumption, which provided a well-defined area of release of the contaminants at the nearest identifiable outfall, was deliberately conservative. Since those calculations, the data have become available for the Culebra and Magenta units separately, as discussed earlier in this report. Comparison of these Figures B-1, B-2, and B-3 with Figures 3-19 shows some of the changes in assignment of the data and the resulting interpretations. For the Culebra the heads are now distributed so that the general trend in the flow is off to the south from the site; the earlier trend was off to the southwest. In addition, it has been established that the Culebra is anisotropic. While Malaga Bend is still the closest outfall, it now appears to be important only for contaminants in Nash Draw. The actual outfall to the south-southwest is unknown, and would be substantially farther away from the site than Malaga Bend. Travel times for fluids were calculated by INTERA and by PNL and are compared by Cole and Bond (1980). Their assumption is that time of travel to Malaga Bend is the important figure. The calculations in this report are for a much shorter distance (8 mi as opposed to <24.3 mi); travel times are shown in Table B-1, where the calculations for this report are given on a mile by mile accounting for three streamlines, namely south-southeast from the center of the site and at the west and east edge of zone three respectively and the calculations for INTERA and PNL are given in total. Few of the original data, except for the porosity which was assumed to be 10%, have been used here.

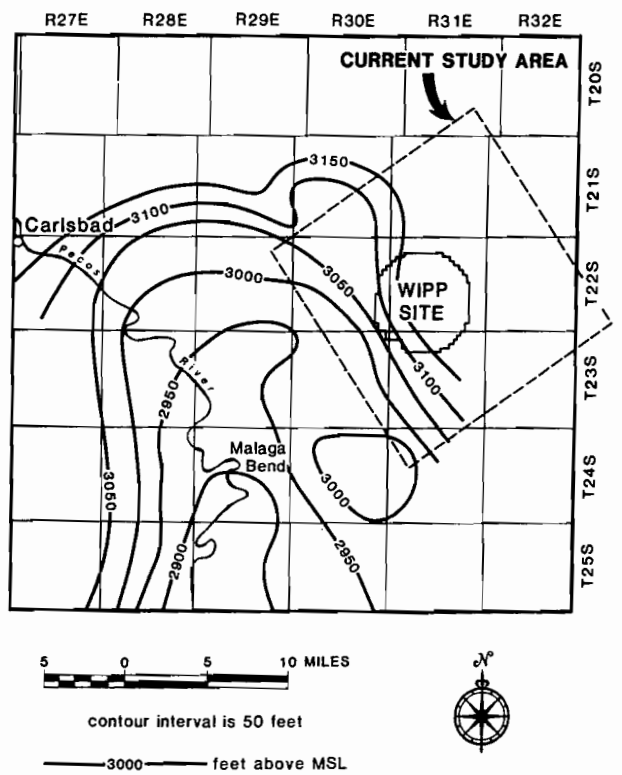

Figure B-1. Hydraulic Potentials (feet above MSL) measured in the Rustler Formation

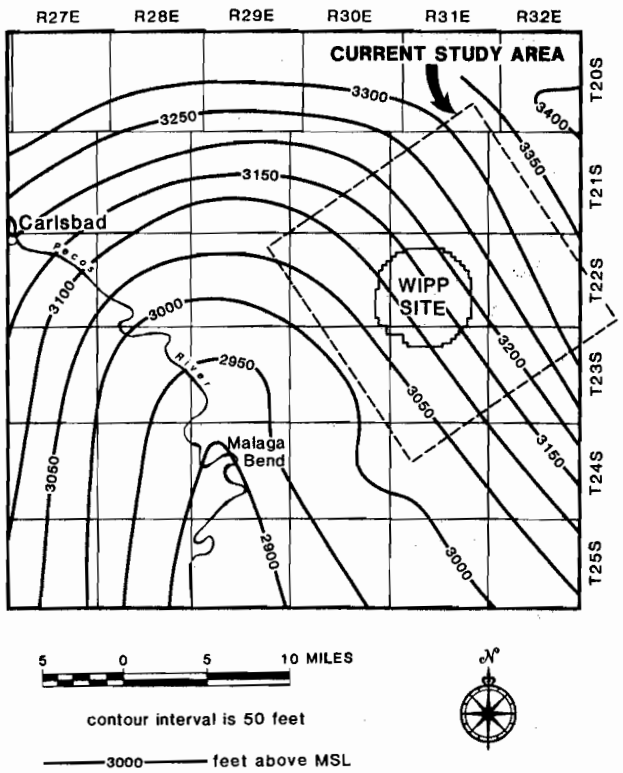

Figure B-2 Calculated Hydraulic Potentials (feet above MSL) for the Rustler Formation

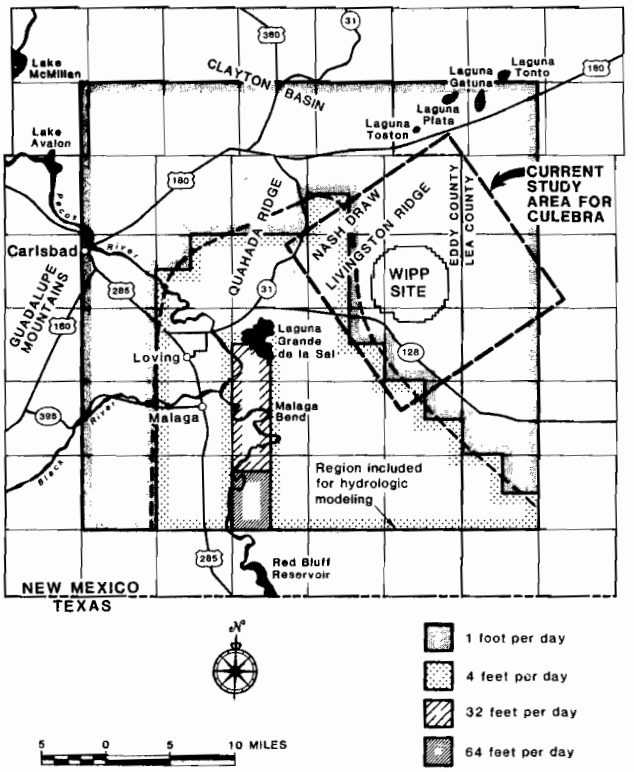

Figure B-3. Hydraulic Conductivities in the Rustler Aquifers

Table B-1. Travel Times for Fluids Along Selected Streamlines

INTERA & PNL Results	Distance (mi)	Time (yr) West Edge of Area 3	Center of Site	East Edge of Area 3
	0–1	7 800 yr	40 000	53 300
	1–2	17 000	19 000	5.2×10^6
	2–3	33 500	46 400	46 400
	3–4	69 500	63 200	63 200
	4–5	830	5 900	5 900
	5–6	950	4 500	4 500
	6–7	700	3 900	3 900
	7–8	650	3 700	3 700
23 mi, 3644.2 yr	8	1.3×10^5	1.87×10^5	5.38×10^6

Travel times were computed from code calculations of particle velocities at nodal points along selected streamlines starting at the left edge, the center, and the right edge of Zone III along a horizontal midline through the repository. Velocities were assumed to apply for a ½ nodal spacing on each side of the node. Then the nodal distance was divided by the maximum nodal velocity to give the minimum travel time. The travel time was reported above on a per mile basis. It is also possible to apply Darcy's law to each node, using the derived head map to obtain gradients and the Tables 1, 2 to get K (hydraulic conductivities) to produce similar estimates. Anisotropy makes the hand calculations somewhat questionable, but the general results are similar.

The results of calculating travel times down streamlines from the centre of the site and from the west and east edges of zone 3 are travel times that exceed the travel time calculated from the FEIS of about 3600 yr for 23 mi by more than an order of magnitude for about one-third that distance. The reasons for the substantial differences in calculated travel times are that there are differences in either values for hydraulic conductivity or for values of the potential gradient; in some cases both differ. The original calculations were bounding and conservative.

APPENDIX C

Test Problem

A test problem was run in order to exercise the code on a reasonably well-defined problem from the field. The point of a test problem is to establish that the various parts of the code are functioning and that results are produced which are consistent with reality. The problem used, which was taken from the literature (Pinder, 1973 and 1974), is that of movement of hexavalent chromium from a disposal pond on Long Island toward Massapequa Creek. The contaminant is in an aquifer below the creek and in part leaks upward to the creek. The simulation requires solution of the steady-state groundwater flow problem and the transient mass-transport problem. The disposal pond is made a constant concentration boundary and the creek is a leaky element discharge area. The outer boundary of the problem is made a Dirichlet boundary for both heads and concentration. Fluid leaves the system by means of the creek, while continuing to carry the same concentration that it has as it arrives at the creek.

The definition of the source based on observation required two separate source concentrations, one of 40 mg/L for the period 1949-1962 and a reduction to 10 mg/L from 1962-1972. The evolution of the contaminant plume is shown in the following set of figures, which may be compared to those in Pinder (1973).

The contaminated plume and location of the leaky elements to the river appear in Figure C-1. Isopleths in these figures are for values of 40, 20, 10, and 1 mg/L in this figure. In the successive Figures C-2, C-3, C-4, the source is assumed reduced 75% and the isopleths are 20, 10, 1 mg/L in these figures. The sequence corresponds to Figure 6 of Reference 11. On all figures the cross hatching indicates the location of the leaky elements corresponding to Massapequa Creek, and the stippled area is the location of the disposal pond.

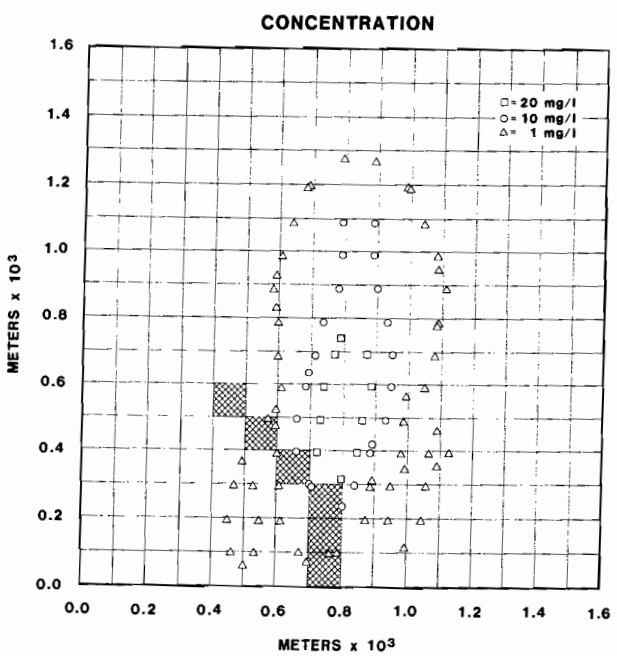

Figure C-1. Concentration of Hexavalent Cr for a Source at the Stippled Element of 40 mg/L With Massopequa Creek at the Cross-Hatched Elements

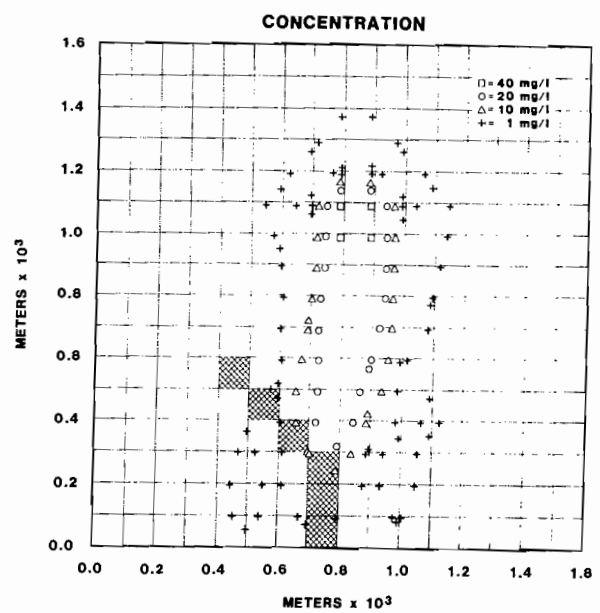

Figure C-2. Concentration of Cr for the Source reduced to 10 mg/L, 1 Yr After the Previous Figure

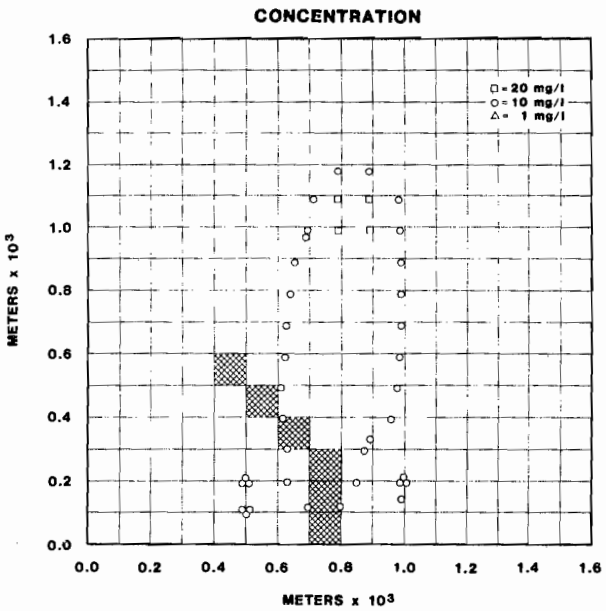

Figure C-3. Concentration of Cr, 4 Yr After Figure A-25

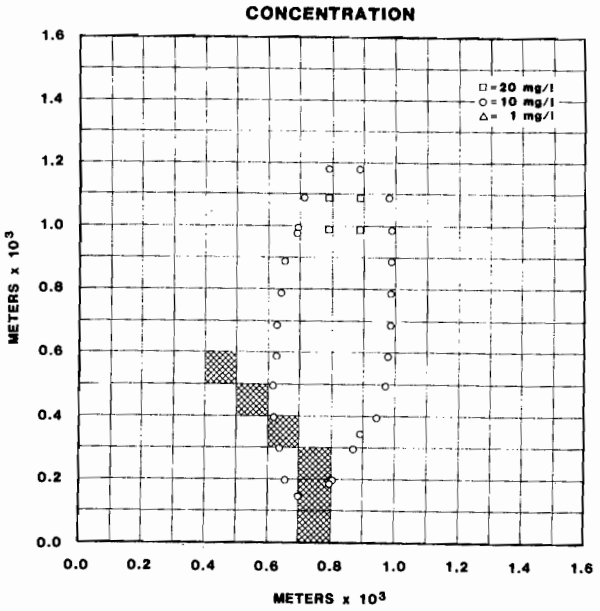

Figure C-4. Concentration of Cr, 7 Yr After Figure A-25

References

[1]S. J. Alweis, *Aquifer tests at H-2 Site*, Hydro Geo Chem, Inc, January 1982.

[2]M. P. Anderson, "Using Models to Simulate the Movement of Contaminants Through Groundwater," *Critical Reviews in Environmental Control 9(2):* 97-156 (1979).

[3]C. R. Cole, F. W. Bond, *Comparison of INTERA and WISAP Consequence Model Application*, PNL-3070/UC-70 (Richland, WA: Pacific Northwest Laboratory, January 1980).

[4]J. B. Cooper and V. M. Glanzman, *Geohydrology of Project Gnome Site, Eddy County, New Mexico*, USGS Prof. Paper 712-A, 1971.

[5]*Final Environmental Impact Statement, Waste Isolation Pilot Plant*, US Department of Energy, October 1980, DOE/EIS-0026, UC-70.

[6]R. A. Freeze, J. A. Cherry, *Groundwater*, P317, (Englewood Cliffs, NJ: Prentice-Hall, Inc.,1979).

[7]D. D. Gonzalez, *Hydrogeochemical Parameters of Fluid-Bearing Zones in the Rustler and Bell Canyon Formations: Waste Isolation Pilot Plant*, SAND83-0210 (Albuquerque, NM: Sandia National Laboratories, 1983).

[8]D. D. Gonzalez, *Groundwater Flow in the Rustler Formation, Waste Isolation Pilot Plant, Southeast New Mexico, Interim Report*, SAND82-1012 (Albuquerque, NM: Sandia National Laboratories, 1983).

[9]INTERA Environmental Consultants, Inc., *Hydrogeological Analysis (1980) in Support of the Waste Isolation Pilot Plant (WIPP) Program*, No. 771-006-01, September 1981.

[10]J. C. S. Long, J. S. Remor, C. R. Wilson, and P. A. Witherspoon, *Porous Media Equivalents for Networks of Discontinuous Fractures*, Water-Resources Research 18, pp 645-658 (1982).

[11]Personal Communication, J. Mercer, US Geological Survey.

[12]J. W. Mercer, *Geohydrology of the Proposed Waste Isolation Pilot Plant Site, Los Medanos Area, SENM*, USGS Water-Resources Investigation, 83-4016, 1983.

[13]G. F. Pinder, *A Galerkin Finite-Element Simulation of Groundwater Contamination on Long Island, New York*, Water-Resources Research 9 (6), pp 1657-1669 (1973).

[14]G. F. Pinder, *Galerkin-Finite Element Models for Aquifer Simulation* (Princeton, NJ: Water Resources Program, Dept of Civil Engineering, Dept of Geological and Geophysical Sciences, Princeton University, 1974).

[15]G. F. Pinder and W. G. Gray, *Finite-Element Simulation in Surface and Subsurface Hydrology* (New York: Academic Press, 1977).

[16]D. W. Powers, S. J. Lambert, S. E. Shaffer, L. R. Hill, and W. D. Weart, *Geological Characterization Report, Waste Isolation Pilot Plant (WIPP) Site, Southeast New Mexico*, SAND78-1596 (Albuquerque, NM: Sandia Laboratories, August 1978).

[17]D. Rai, R. J. Serne, and D. A. Moore, "Solubility of Plutonium Compounds and Their Behavior in Soils," *Soil Science Soc of Am J, 44*, p490 (1980).

[18]D. Rai and J. L. Swanson, "Properties of Plutonium (IV) Polymer of Environmental Importance," *Nucl Technol, 54*: 107-112 (1981).

[19]D. Rai and J. L. Ryan, "Crystallinity and Solubility of Pu (IV) Oxide and Hydrous Oxide in Aged Aqueous Suspensions, " *Radiochimica Acta 30:* 213-216 (1982).

[20]D. Rai, R. J. Serne, and J. L. Swanson, "Solution Species of Plutonium in the Environment," *J Environmental Quality, 9:* 417-420 (1980).

[21]K. R. Rushton, S. C. Redshaw, *Seepage and Groundwater Flow* (New York: John Wiley & Sons, 1979).

[22]T. D. Streltsova-Adams, *Well Hydraulics in Heterogeneous Aquifer Formations*, pp 357-423, in Advances in Hydroscience, Vol II (1978).

[23]J. J. Ward, G. Water, and D. D. Gonzalez, *Aquifer Tests to Determine the Principal Components of Transmissivity in the Culebra Dolomite at Hydropads H-4, H-5, and H-6 (WIPP), Southeast New Mexico*, SAND83-7009 (Albuquerque, NM: Sandia National Laboratories, 1983).

DISTRIBUTION:

US Department of Energy, HQ (2)
Office of Nuclear Waste Management
Attn: B. Bennett, Director,
Division of Waste Isolation
Washington, DC 20545

US Department of Energy, HQ (2)
Office of Defense Waste & By-Products
Attn: G. Oertel, Director (NE-320)
L. Harmon, Program Manager (WIPP)
Washington, DC 20545

US Department of Energy (4)
Albuquerque Operations
Attn: R. Romatowski (For: D. Schueler)
J. M. McGough, Manager,
WIPP Project Office (2)
D. Jackson, Director, Public Affairs Division
PO Box 5400
Albuquerque, NM 87185

DOE WIPP Project Office, Carlsbad
Attn: W. Jebb, Site Manager
PO Box 2078
Carlsbad, NM 88221

US Department of Energy
c/o Battelle Office of Nuclear Waste Isolation
Attn: J. O. Neff
505 King Avenue
Columbus, OH 43201

Battelle Memorial Institute (4)
Office of Nuclear Waste Isolation
Attn: S. Goldsmith, Manager (3)
ONWI Library
505 King Avenue
Columbus, OH 43201

Battelle Memorial Institute
Project Management Division
Attn: N. Carter, General Manager
505 King Avenue
Columbus, OH 43201

Bechtel National, Inc. (2)
Fifty Beale Street
Attn: E. Weber, Jr.
D. Roberts
PO Box 3965
San Francisco, CA 94119

D'Appolonia Consulting Engineers
Attn: D. Shukla
2340 Alamo, SE
Albuquerque, NM 87106

Westinghouse Electric Corporation (4)
Attn: R. K. Brown
C. Little
R. Jones (TSC)
C&C File
PO Box 40039
Albuquerque, NM 87196

Vanderbilt University
Department of Environmental and
Water Resources Engineering
Attn: F. L. Parker, Chairman
Nashville, TN 37235

Stanford University
Department of Geology
Attn: K. B. Krauskopf, Vice Chairman
Stanford, CA 94305

K. P. Cohen
Consultant
928 N. California Avenue
Palo Alto, CA 94303

University of California at Berkeley
Dept. of Material Sciences and Engineering
Attn: N. G. W. Cook
Hearst Mining Building, #320
Berkeley, CA 94720

F. M. Ernsberger
250 Old Mill Road
Pittsburgh, PA 15238

Pennsylvania State University
Department of Hydrogeology
Attn: R. R. Parizek
University Park, PA 16802

D. A. Shock
233 Virginia
Ponca City, OK 74601

Florida State University
Department of Oceanography
Attn: J. W. Winchester
Tallahassee, FL 32306

DISTRIBUTION (Cont):

J. T. Holloway
Senior Staff Officer
2101 Constitution Avenue, NW
Washington, DC 20418

WIPP Public Reading Room
Atomic Museum, Kirtland East AFB
Attn: G. Schreiner
Albuquerque, NM 87185

WIPP Public Reading Room
Carlsbad Municipal Library
Attn: L. Hubbard, Head Librarian
101 S. Hallagueno St
Carlsbad, NM 88220

Thomas Brannigan Library
Attn: D. Dresp, Head Librarian
106 W. Hadley St
Las Cruces, NM 88001

Roswell Public Library
Attn: N. Langston
301 N. Pennsylvania Avenue
Roswell, NM 88201

Hobbs Public Library
Attn: M. Lewis, Librarian
509 N. Ship St
Hobbs, NM 88248

State of New Mexico (2)
Environmental Evaluation Group
Attn: R. H. Neill, Director
320 Marcy Street
PO Box 968
Santa Fe, NM 87503

NM Department of Energy & Minerals (2)
Attn: P. Biderman, Secretary
K. LaPlante, Librarian
PO Box 2770
Santa Fe, NM 87501

Mining & Minerals Division
Attn: E. Kelley, Director
525 Camino de los Marquez
Santa Fe, NM 87501

New Mexico State Library
Attn: I. Vollenhofer
PO Box 1629
Santa Fe, NM 87503

New Mexico Tech
Martin Speer Memorial Library
Campus Street
Socorro, NM 87801

University of New Mexico
Reference Department
Zimmerman Library
Attn: Z. Vivian
Albuquerque, NM 87131

USGS, Water Resources Division (2)
Attn: J. W. Mercer
505 Marquette, NW
Western Bank Bldg, #720
Albuquerque, NM 87102

USGS, Special Projects Branch (2)
Federal Center, Bldg 25
Attn: R. P. Snyder
Denver, CO 80225

New Mexico Bureau of Mines (2)
and Mineral Resources
Attn: F. E. Kottlowski, Director
Socorro, NM 87801

Klaus Kuhn
Gesellschaft fuer Strahlen-und
Umweltforschung MBH Muenchen
Institut fuer Tieflagerung
Berliner Strasse 2
3392 Clausthal-Zellerfeld
FEDERAL REPUBLIC OF GERMANY

Klaus Eckart Maass
Hahn-Meitner-Institut fuer Kernforschung
Glienicker Strasse 100
1000 Berlin 39
FEDERAL REPUBLIC OF GERMANY

DISTRIBUTION (Cont):

Michael Langer
Bundesanstalt fuer Geowissenschaften
und Rohstoffe
Postfach 510 153
3000 Hannover 51
FEDERAL REPUBLIC OF GERMANY

Helmut Rothemeyer
Physikalisch-Technische
Bundesanstalt
Bundesalle 100
3300 Braunschweig
FEDERAL REPUBLIC OF GERMANY

US Nuclear Regulatory Commission (3)
Division of Waste Management
Attn: M. Bell
Mail Stop 69755
Washington, DC 20555

Rolf-Peter Randl
Bundesministerium fuer Forschung
und Technologie
Postfach 200 706
5300 Bonn 2
FEDERAL REPUBLIC OF GERMANY

6300 R. W. Lynch
6330 W. D. Weart
6331 A. R. Lappin
6332 L. D. Tyler
6332 Sandia WIPP Central Files (2)
8424 M. A. Pound
3141 D. K. Brown, (Actg) (5)
3151 W. L. Garner (3)
3154-3 C. H. Dalin (25)
For DOE/TIC (Unlimited Release)